Journal of Applied Physics

Raman spectroscopy for carbon nanotube applications

Cite as: J. Appl. Phys. **129**, 021102 (2021); https://doi.org/10.1063/5.0030809
Submitted: 24 September 2020 • Accepted: 18 December 2020 • Published Online: 11 January 2021

A. Jorio and R. Saito

Journal of Applied Physics TUTORIAL scitation.org/journal/jap

Raman spectroscopy for carbon nanotube applications

Cite as: J. Appl. Phys. **129**, 021102 (2021); doi: 10.1063/5.0030809
Submitted: 24 September 2020 · Accepted: 18 December 2020 ·
Published Online: 11 January 2021

A. Jorio[1,a)] and R. Saito[2,b)]

AFFILIATIONS

[1]Physics Department, Universidade Federal de Minas, Belo Horizonte, MG 31270-901, Brazil
[2]Department of Physics, Tohoku University, Sendai 980-8578, Japan

Note: This paper is part of the Special Topic on Physics and Applications of Nanotubes.
[a)]**Author to whom correspondence should be addressed:** adojorio@fisica.ufmg.br
[b)]**Electronic mail:** rsaito@flex.phys.tohoku.ac.jp

ABSTRACT

The use of Raman spectroscopy for carbon nanotube applications is presented here as a tutorial review. After introducing the relevant basic aspects of Raman spectroscopy of graphene-related materials, we will discuss how to use the Raman spectral features for practical purposes of controlling and characterizing nanotube properties relevant for applied materials and devices. Advanced techniques with potential to enhance the relevance of Raman spectroscopy application in the carbon nanotube field are also presented.

I. INTRODUCTION

The application of carbon nanotubes (CNTs) to advanced materials and devices has been broadly explored, maturing already in the first decade of the 21st century.[1–8] Examples are found in many fields, including reinforcement fibers,[3,9] electronics,[10,11] microelectronics,[12] electron sources,[13] field emission displays,[14] single-photon emitter,[15,16] composites for electrical applications,[17] flexible electronics,[18] super-capacitors,[19–21] organic light-emitting diodes,[22] and solar cells,[23] among others. It also deserves to mention applications of biomedicine and health,[24,25] including removal of contaminants in drinking water,[26] tissue engineering,[27] and biomedical[28] and biosensing[29,30] applications, for instance, CNT-based sensors for detection of dengue virus NS1 protein[31] and tumor targeting.[32]

Many applications rely, of course, on the well-established outstanding mechanical, thermal, electronic, and optical properties of CNTs,[2,5,33–35] which have both aspects shared with all sp^2 related carbons, like graphite, graphene, and amorphous carbon. The application also relies on unique properties of a CNT, which come from the special one-dimensional character of CNTs that is enriched by their helical structure, as defined by diameter (d_t) and chiral angle (θ), with an uncountable number of isomers specified by two integer (n, m).[33] Besides, carbon nanotube application also depends strongly on aspects that can vary among carbon nanotube-based materials, among CNT-based devices, and here is where Raman spectroscopy has been established as a commonly used, standard tool.

Raman spectroscopy (RS), in which we observe the inelastic scattering of light, is a technique that carries two important and unique aspects that make it highly relevant for the characterization of advanced materials and devices. First, since RS generally utilizes visible light as a probe, RS is a non-contact and non-invasive characterization tool that can be operated at both ambient (room temperature and in air) and controlled environment conditions, applied directly on any material or device with optical access. This operation is safe for the user and it does not disturb much the intrinsic properties of the measured material. Second, RS has access to the fine electric and vibrational properties of the materials with a high energy resolution, being able to distinguish energy resolution down to μeV, a resolution generally much superior to any other nanotechnology technique based on electron microscopy such as electron energy-loss spectroscopy (EELS), scanning probe spectroscopy (SPS), or even other optical techniques relying on less well-defined energy levels, such as photoluminescence or infrared reflection spectroscopy. This sensitivity makes RS applicable not only to characterize the devices but also to serve as the relevant metric of a CNT-based sensor.

For the specific case of single-wall carbon nanotubes (SWNTs) and also other graphene-related materials, RS has an extra aspect

that makes it even more powerful, which is the highly efficient and selective resonance effects.[36] The resonance effect makes it possible to measure one isolated carbon nanotube by RS[37] and makes it possible to obtain information from the vibrational properties that are usually Raman inactive.[38] Accessing phonons that are Raman inactive (e.g., phonons in the interior of the Brillouin zone) is important to characterize several static and dynamic properties of a solid or a molecule, but they are generally accessible only by inelastic neutron or x-ray scattering or EELS, which require expensive infrastructure and a single crystal of material, which is not suitable for the application for nanoscale devices.

The motivation of the present article comes from the fact that RS can say much more than phonon frequency of the device, such as characterizing strain, doping, defects, and interactions with the surrounding materials. Further, we could get much information by adopting advanced techniques for CNT-based materials and devices with keeping applicability to the industrial perspective. Following this motivation, this work is structured as follows: in Sec. II, we introduce the fundamentals of Raman spectroscopy in graphene and carbon nanotubes, which is necessary to understand its applications. In Sec. III, we discuss the applications of Raman spectroscopy with a focus on the following: the use of the radial breathing mode ($\sim$50$-$350 cm^{-1}) to characterize synthesis and CNT sorting in Sec. III A; the usage of the G ($\sim$1584 cm^{-1}) and G′ ($\sim$2600$-$2800 cm^{-1}) bands for strain, doping, and isotope characterization in Sec. III B; and the usage of defect-induced bands (focus on the D band, $\sim$1300$-$1400 cm^{-1}) for defect identification and quantification in Sec. III C. Notice the G′ is more commonly referred to as the 2D band in the most recent graphene literature, after Ferrari *et al.*,[39] although it is not an overtone of the D peak.[40] Section III D closes this section with considerations about the general applicability of these concepts with a focus on carbon nanotube composites. In Sec. IV, our discussion addresses how Raman spectroscopy can be used in Raman intensity mapping, which provides not only sample imaging but also carries local functional information. The discussion starts with the usual micro-Raman imaging in Sec. IV A, followed by examples of the use of tip-enhanced Raman spectroscopy (TERS) for nano-Raman imaging in Sec. IV B, finishing with comparison to other techniques in Sec. IV C. Finally, in Sec. V, we introduce, in a tutorial style, some complementary advanced techniques, with potential to help generating novel applications: electro-chemical doping (Sec. V A), circular dichroism (Sec. V B) and helicity-changing Raman spectroscopy using circularly polarized light (Sec. V C), and coherent phonon spectroscopy (Sec. V D). Some symmetry aspects related to group theory (GT) are utilized, and for a review on GT applied to solid state physics, see Ref. 41, or for GT specifically on carbon nanotubes, see Ref. 42. This Tutorial ends in Sec. VI where we present our conclusions and future perspectives for RS-based CNT applications.

Finally, it is important to stress that this article is limited in two ways. First, it focuses more on practical applications than on the fundamental concepts of Raman spectroscopy applied to carbon nanotubes; second, the authors try to cover the field, but generally we focus on the subjects that we have mainly contributed. To overcome these two limitations, we point the readers to other excellent articles and reviews that can be found in the literature, written by other experts in the field who contributed enormously to the advance of the concepts and applications in this field. Several references will be given along our review, but here, for instance, we can indicate Refs. 43–55.

II. GENERAL ASPECTS OF THE RAMAN SPECTRA FROM SWNTs

When a material is perturbed by monochromatic radiation, usually an incident laser of wavelength λ_i, the material responds by emitting light at the same energy (elastic scattering, $\lambda_s = \lambda_i$) and at shifted energies (inelastic scattering, $\lambda_s \neq \lambda_i$). The Raman spectroscopy, which offers a spectral fingerprint of a material, is a measurement of the inelastically scattered light emitted by the material. The Raman spectral signature for the material is composed by a set of specific wavelengths (λ_s^q), associated with the interaction of the incident light with a given lattice vibrational mode ν_q as a function of the wave vector q. The Raman shift of a given mode ν_q is the change of energy in the inelastically scattered light with respect to that of the incident light. The Raman spectrum is a plot of the intensity of the scattered light, $I_s[\Delta(1/\lambda_{i,s})]$, as a function of the Raman shift $\Delta(1/\lambda_{i,s})$, which is given by

$$\Delta(1/\lambda_{i,s}) = \frac{10^7}{\lambda_s} - \frac{10^7}{\lambda_i}, \tag{1}$$

where $\lambda_i(\lambda_s)$ is the wavelength of the incident (scattered) light given in nm and $\Delta(1/\lambda_{i,s})$ is the wavenumber given in units of cm^{-1} (1 eV = 8065 cm^{-1}). It is noted that cm^{-1} is used as an energy in Raman spectroscopy. The peak of Raman spectra at $\Delta(1/\lambda_{i,s=q})$ corresponds to the elementary excitation of a specific mode ν_q of the material, which is called a Raman active mode. The plot of $I_s\left[\Delta(1/\lambda)_{i,s}\right]$ is generated by a Raman spectrometer, which is usually composed by a light dispersion grating and a charged coupled device (CCD) camera. The scattered light is dispersed by the grating to a different direction toward the CCD, and the spectrometer software converts CCD pixel position into $\Delta(1/\lambda_{i,s})$ in cm^{-1}, thus building the $I_s[\Delta(1/\lambda_{i,s})]$ plot. Examples are given in Fig. 1, where at almost zero Raman shift would be observed the $\lambda_s \approx \lambda_i$ peak, but the elastic scattering is blocked by a notch filter, while the other peaks at $\lambda_s \neq \lambda_i$ compose the Raman signature of the materials.

When we characterize the Raman spectra of a SWNT, it is important to investigate the similarities and differences of the Raman spectra among the graphene-related structures. Figure 1 shows the Raman spectra of several graphene-related materials. What all these materials have in common is an atomic structure majorly defined by carbon atoms connected to each other by sp^2 carbon bonds, and this is why all the Raman spectra of other atoms or chemical bonds would appear at different Raman shifts. The special/general aspects of the Raman spectra from sp^2 carbons are listed below:

- RBM: Carbon nanotubes have a unique Raman-active mode around $\omega_{RBM} \sim 100-200\,\text{cm}^{-1}$, not present in any other graphene-related structure, which is the so-called radial breathing mode (RBM, see SWNT spectrum in Fig. 1). This vibrational mode exists because of the cylindrical shape of a nanotube, in

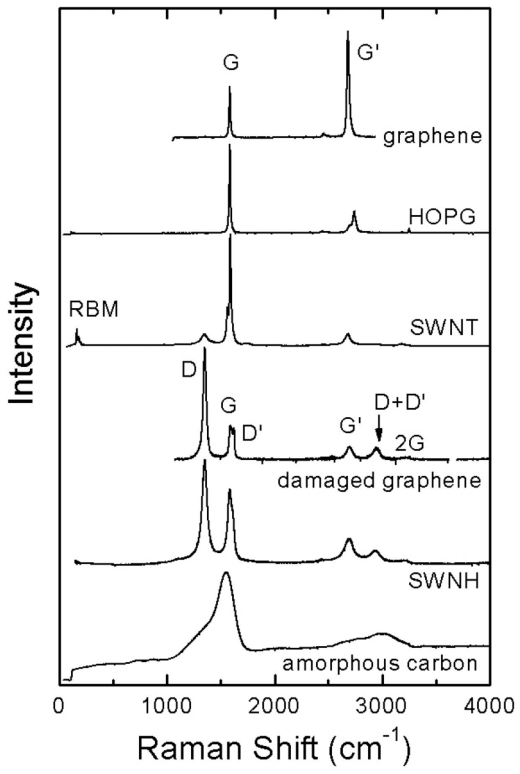

FIG. 1. Exemplary Raman spectra of, from the top to the bottom: pristine graphene, highly oriented paralytic graphite (HOPG), single-wall carbon nanotubes (SWNTs), graphene damaged by ion bombardment, single-wall carbon nanohorns (SWNHs), and amorphous carbon grown by chemical vapor deposition. Evidenced are the radial breathing modes (RBMs), the defect-induced peaks (D, D′ and the combination D + D′), the G mode, and the overtones G′ (or 2D) and 2G. Reproduced with permission from Dresselhaus *et al.*, Nano Lett. **10**, 751–758 (2010).[240] Copyright 2010 American Chemical Society.

which the radius of the nanotube is oscillating (like the tube breathing). The RBM is an out-of-plane bond-stretching mode whose frequency is inversely proportional to the diameter of a SWNT, d_t, as discussed in Sec. III A.

- G band: The G band is in-plane bond stretching mode of the C—C bonds in the hexagonal lattice whose Raman peak appears at $\sim$1585 cm^{-1}. The G band commonly appears in all the sp^2 carbon materials (see Fig. 1). In pristine graphene, the G band is composed by a single Lorentzian peak.[58] In a SWNT, the G band splits into G^+ and G^- peaks due to the strain effect, which is related to the curvature and/or due to electron–phonon coupling in a SWNT, as it will be discussed in Sec. III B. For defective carbon materials, the G band broadens due to bond in-homogeneity and shortening of phonon lifetime, as discussed in Sec. III C.
- G′ band (or 2D band[40]): Another peak present in the spectra of most sp^2 carbon materials is the so-called G′ band, appearing at $\omega_{G'} \sim 2700$ cm^{-1} (see Fig. 1) for a 514 nm laser (the exact frequency of the G′ peak depends on the excitation laser energy[38,59–62]). The G′ peak is related to the Raman scattering due to a vibrational mode characterized by the breathing of six carbons pertaining to a hexagon in the hexagonal lattice of graphene. The frequency for the breathing vibration is actually half of the observed value ($\sim$1350 cm^{-1}), but the hexagon-breathing mode is not Raman active in first-order Raman scattering,[63] being observable only as an overtone, which is Raman allowed. In pristine graphene, this G′ band is composed by a single Lorentzian peak, while in all other sp^2 carbon structures, the line shape is deformed due to several effects, as is discussed in Sec. III B.
- D band: if the hexagonal sp^2 network exhibits a defect, the first-order component of the hexagon-breathing mode is activated combined with an elastic scattering of a photo-excited electron by the defect, as a double-resonance Raman peak (see below),[64,65] which appears at $\omega_D \sim 1350$ cm^{-1} and it is called the D band (see the three bottom spectra of Fig. 1). Notice the presence of a sharp D peak for the spectra of damaged graphene and single-wall nanohorns (SWNHs). When the structure is too damaged, like in amorphous carbon (the bottom most spectrum in Fig. 1), the D and G bands are overlapped each other by broadening. Other defect-induced peaks are also activated (e.g., D′ and D+D′ in Fig. 1), and they are usually weak in intensity when compared to the D band. Notice the G′ band is an overtone of the D mode, and for this reason it is also called 2D in the literature, although it has no direct relation to defects. The D band is discussed in Sec. III C.
- Double-resonance Raman peaks: Finally, all graphene-related materials exhibit several other peaks (IFM, D', M, ItoLA, etc.), which are related to second-order, two-phonon (or one-phonon and one-elastic scattering) double resonance Raman processes involving the scattering of the photo-excited electron in the Brillouin zone by a non-zone-center ($q \neq 0$) phonon[38,66] [e.g., IFM peaks in Fig. 2(b)], which will not be properly discussed in this article because they are usually too weak and not commonly utilized on applications. It is noted that G' and D are also double resonance Raman peaks. The double-resonance phenomenon was introduced by Thomsen and Reich[67] to explain the D band and further extended to other Raman features by Saito *et al.*[38] Reviews focusing on the phenomena from these and other authors, including pictures for the scattering diagrams can be found in the literature, see, e.g., Refs. 48, 66, and 68–72.

Having established the general aspects of the Raman spectra from graphene-related structures, let us focus our attention on the Raman spectra of (a) a metallic (top) and a semiconducting (bottom) isolated SWNT dispersed on a silicon substrate and (b) SWNT bundles as shown in Fig. 2. The main features (RBM, D, G, and G′) are highlighted in (a), while the peaks marked by * come from the substrate. Also highlighted in Fig. 2 are some small features (named M, iTOLA, or IFM) that are double-resonance Raman peaks.[66,73,74]

In Fig. 2(a), we can see that the spectral width of the G band of a SWNT is broader for metallic SWNT than that of a semiconducting SWNT. The broadening is understood by the Kohn anomaly effect for a metallic SWNT, as is discussed in detail in Secs. III B and V A.[75–77] In Fig. 3(a), we schematically show the perturbation for a phonon in the Kohn anomaly effect in which a

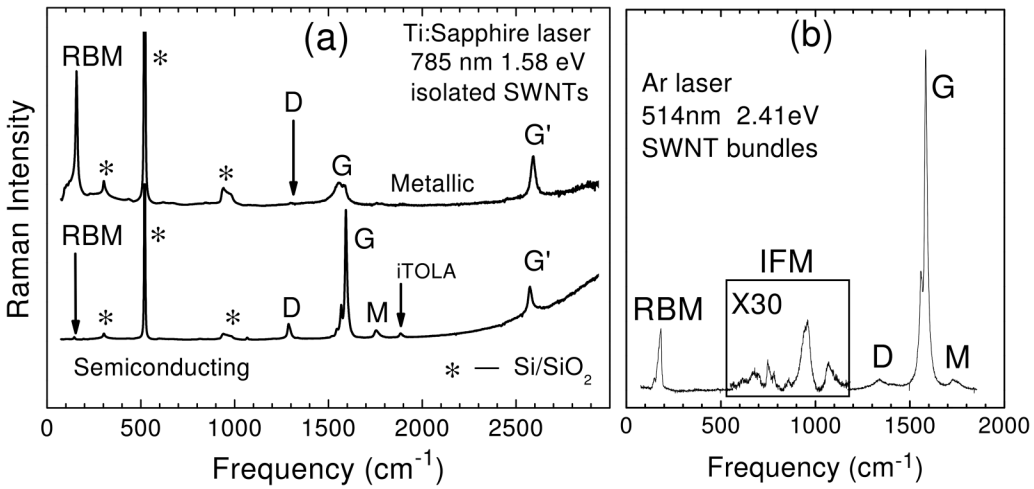

FIG. 2. Raman spectra from carbon nanotubes: (a) isolated carbon nanotubes deposited on an oxidized silicon (Si/SiO_2) substrate. The top spectrum stands for a metallic SWNT, while the bottom one stands for a semiconducting SWNT (see Ref. 56). Reproduced with permission from Dresselhaus *et al.*, J. Phys. Chem. C **111**, 17887–17893 (2007).[241] Copyright 2007 American Chemical Society. (b) Bundled SWNT sample. The inset named IFM (intermediate frequency modes) is magnified in intensity by 30× to highlight the small intensity peaks (see Ref. 57). The main Raman features of SWNTs are labeled, and the peaks of the Si/SiO_2 substrate are marked with a "*." Reproduced with permission from Dresselhaus *et al.*, Philos. Trans. A Math. Phys. Eng. Sci. **362**, 2311–2336 (2004).[242] Copyright 2004 Royal Society.

phonon with the energy $\hbar\omega_0$ virtually excite an electron–hole pair in a metallic SWNT by electron–phonon interaction and the pair recombines back to a phonon from the left to the right of the figure. The second-order perturbation for a phonon by electron–phonon interaction makes the phonon energy lower and the lifetime of the phonon short, which gives the softening and broadening of the Raman spectra in the metallic SWNT in Fig. 2, respectively. A semiconducting carbon nanotube does not show such Kohn anomaly effect because the energy gap between the valence and conduction bands is larger than the phonon energy, and the process displayed in Fig. 3(a) does not occur. Back to the metallic SWNT, part of the process is suppressed by doping, as

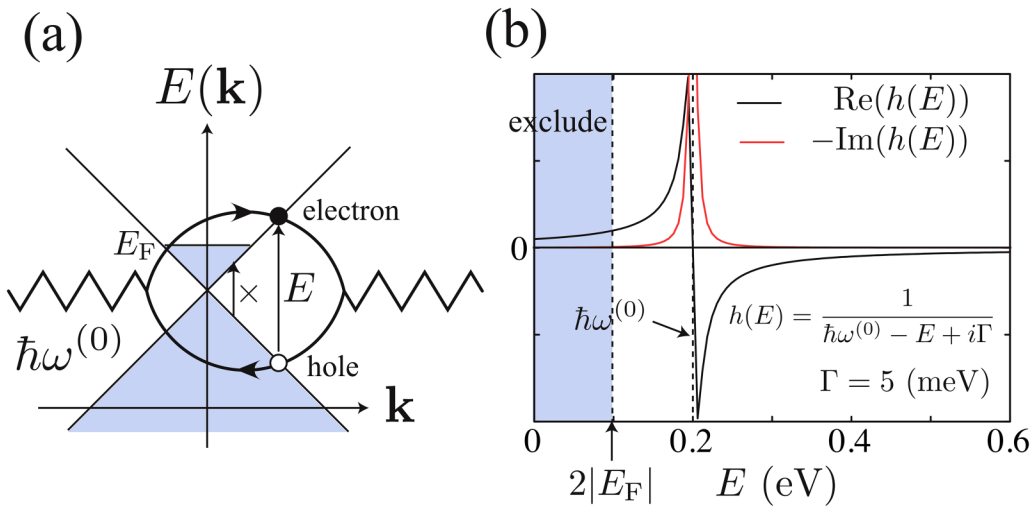

FIG. 3. (a) An intermediate e–h pair state is excited by a phonon in the second-order perturbation, making the optical phonon modes soft (the Kohn anomaly effect). The phonon mode is denoted by a zigzag line, and an e–h pair is represented by a loop. The low energy e–h pair satisfying $0 \le E \le 2|E_F|$ is forbidden at zero temperature by the Pauli exclusion principle. (b) The energy correction to the phonon energy by an intermediate e–h pair state. The sign of the correction depends on the energy of the intermediate state as $h(E)$. Reproduced with permission from Sasaki *et al.*, Phys. Rev. B **77**, 245441 (2008).[142] Copyright 2008 American Physical Society.

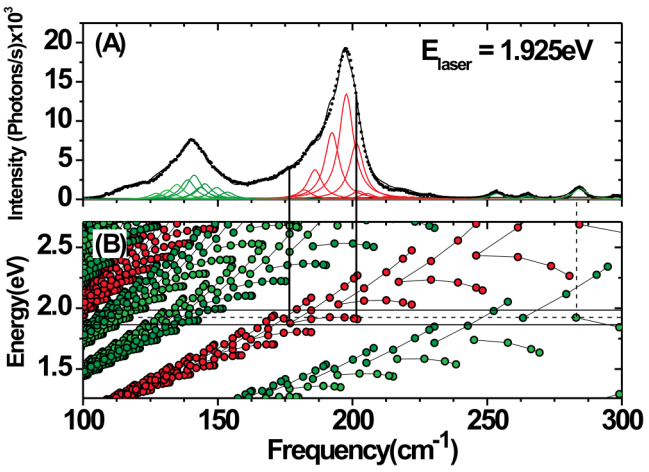

FIG. 4. (a) Raman spectrum (bullets) obtained with a 644 nm laser line. The spectrum was fitted by using 34 Lorentzians (curves under the spectra) and the solid line is the fitting result. (b) The Kataura plot for SWNTs, where each bullet represents one optical transition energy for a given SWNT (see also Fig. 5). The vertical dashed line marks the laser energy used in (a), and the solid line marks the approximate RBM resonance window. Reproduced with permission from the supplementary information of Araujo *et al.*, Physica E **42**, 1251–1261 (2010). Copyright 2010 Elsevier.

shown by the "×"-labeled arrow in Fig. 3(a), which happens for phonon excitation energies up to twice of the Fermi energy, $2|E_F|$, which is shown by the blue shaded region in Figs. 3(a) and 3(b). In Fig. 3(b), we show the definition of energy denominator $h(E)$ of the perturbation. The change of the phonon frequency [Re($h(E)$)] and the spectral width [Im($h(E)$)] of the G band is used for characterizing the doping concentration.

The most important influence of the one-dimensional (1D) electronic structure of a SWNT on their Raman spectra is the resonance effect. Resonance Raman scattering happens when either the incident or the scattered light matches an optical transition energy, causing an enhancement of the Raman signal by many orders of magnitude (typically 10^3). Therefore, the Raman spectra from a CNT sample are dominated by the SWNTs in resonance. This fact is exemplified in Fig. 4, which shows the RBM Raman spectrum of a carbon nanotube bundle composed by SWNTs [Fig. 4(A)] within the transition energy window (1.925 ± 0.050 eV by two solid lines), as shown in Fig. 4(B). The RBM frequency depends on tube diameter d_t (see Sec. III A), and each Lorentzian peak utilized to fit the RBM spectrum represents the RBM peak from one resonant SWNT d_t. However, although the distribution in diameter is homogeneous, the RBM spectrum is obtained only by resonant SWNTs. In Fig. 4(B), all the optical transition energies for all SWNTs are plotted as a function of RBM frequency (ω_{RBM}), which is called the Kataura plot. The Kataura plot is usually displayed as a function of d_t, but here we plot the transition energy as a function of ω_{RBM}, since $\omega_{RBM} \propto 1/d_t$, see Sec. III A. The horizontal dashed line marks the laser excitation energy (E_{laser}). Notice that for each bullet (optical transition) inside the RBM resonance window (the energy region between the two solid lines), there is one Lorentzian in the RBM spectrum in Fig. 4(A).

One can now use the RBM spectra to experimentally determine the Kataura plot, as shown in Fig. 5. On the left, we have the Kataura plot, now as a function of diameter, and on the right a Raman intensity map of the resonance RBMs as a function of

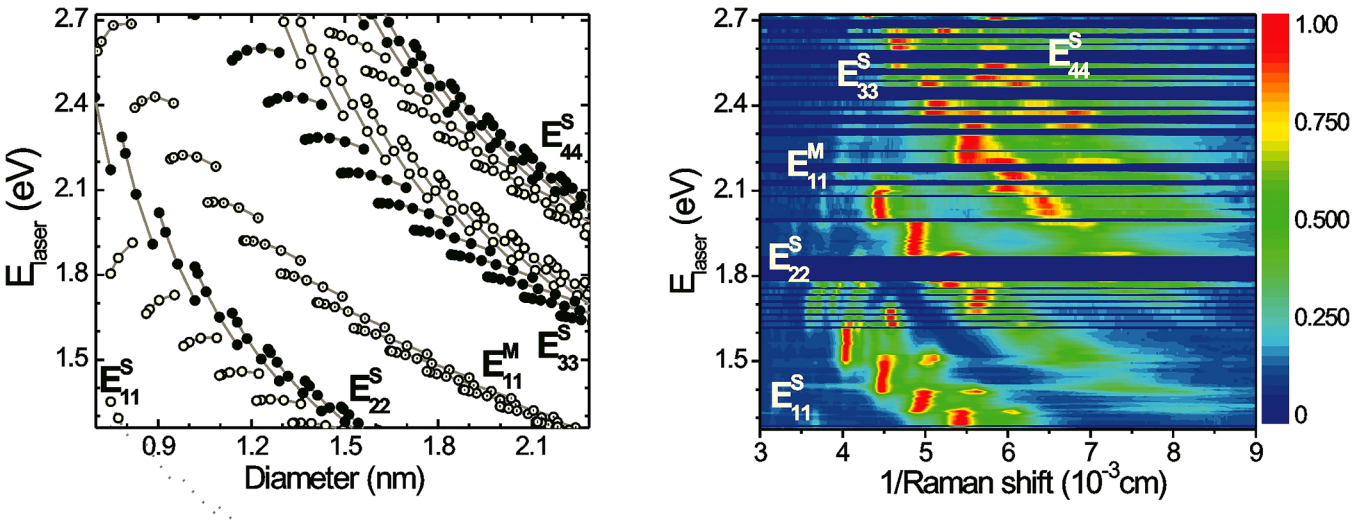

FIG. 5. Left: The Kataura plot for SWNTs. Each carbon nanotube has a set of optical transitions, which are named E_{ii}, where $i = 1, 2, 3, \ldots$. The S and M superscripts stand for semiconducting and metallic SWNTs, respectively. For semiconducting SWNTs, an electronic effect named trigonal warping divides E_{ii} in type I and type II semiconducting SWNTs, indicated by the open and filled bullets, respectively. Right: RBM resonance Raman map. The color code indicated the relative Raman intensity. Reproduced with permission from Araujo *et al.*, Phys. Rev. Lett. **98**, 067401 (2007). Copyright 2007 American Physical Society.

$1/\omega_{RBM}$, which is obtained from the Raman spectra of a carbon nanotube bundle by changing the E_{laser} from 1.3eV to 2.7 eV. This procedure is utilized to fully understand the photophysics of SWNTs, by accurately describing the optical transition energies, including effects of tube curvature and many-body effects, such as electron–electron repulsion and electron–hole attraction (formation of excitons).[78–81]

III. APPLICATIONS OF RAMAN SPECTROSCOPY

In the application of Raman spectroscopy to characterize carbon nanotubes, the first general aspect is the classification of nanotubes when addressing (1) small diameter few-walls carbon nanotubes—single-wall (SWNT) and double-wall (DWNT) with smaller diameter tubes below 2 nm—and (2) larger diameter tubes ($d_t > 2\,nm$) and many walls, more specifically multi-wall carbon nanotubes (MWNTs). In case (1), it is possible to distinguish the specific SWNT structure, i.e., the diameter (d_t) and the chiral angle (θ), thus defining the chiral vector by the two integers (n, m).[33] In case (2), the properties of many (n, m) SWNTs with a large d_t are too similar to characterize. Therefore, for small diameter tubes, each (n, m) SWNT (or part of a DWNT) has a unique and characteristic Raman spectral signature, while for large diameter tubes, the results are just the Raman spectral characteristic in the limit of larger diameter tubes ($d_t \to \infty$) or graphene. For this reason, here we focus on the properties of small diameter tubes, and the characterization of, for example, MWNTs, can be considered a rational extension. For an in-depth description of the physics behind the Raman spectra of carbon nanotubes, see Ref. 36.

A. Radial breathing mode and synthesis/sorting characterization

One of the important aspects for carbon nanotube application is the controlled synthesis and the further structural sorting, to enable engineering applications out of well-defined carbon nanotube properties, as already discussed in several review articles in the literature.[82–93] Since the radial breathing mode (RBM) is a unique vibration among graphene-related materials, and it is unique among specific SWNTs, the RBM relative intensity can be used to describe the carbon nanotube content in a sample.

Raman spectroscopy has been broadly utilized to determine the (n, m) content in a sample. Examples are DNA-wrapped CoMoCAT sample dispersed in aqueous solution,[94] HiPco sample dispersed in aqueous solution with SDS surfactant,[95] carpet-like alcohol-assisted CVD,[79] phosphorus-doped SWNTs,[96] 0.4 nm diameter SWNTs grown inside the pores of zeolite crystals,[97] among others. In the case of CoMoCAT samples, it was shown that the RBM resonance Raman mapping can be used to differentiate the (n, m) contents found in the as-grown purified sample, the SWNT+SDS solution sample, and the SWNT+SDS precipitate sample.[98]

DWNTs are also interesting samples with a rich RBM resonance Raman map.[99,100] A very special technique of separation has been shown recently,[101] where the authors sort DWNTs by semiconducting (S) or metallic (M) constituent tubes for the inner and outer walls of a DWNT. The electronic coupling between the inner and outer walls was used to alter the surfactant coating around each of the DWNT types, and an aqueous-gel permeation was then used to separate them. The enriched DWNT fractions were then transferred into either chlorobenzene or toluene using the copolymer PFO–BPy to yield the four inner@outer combinations of M@M, M@S, S@M, and S@S. The sorting is characterized by the RBM resonance Raman mapping, as shown in Fig. 6.

To rationalize this type of analysis, one has to define the relationship between the RBM properties and the (n, m) structural indices. Since we have two indices, we need to define two spectral information, which are the RBM frequency (ω_{RBM}) and the RBM intensity. The RBM intensity becomes the maximum when the excitation laser matches the (n, m)-dependent, optical transition energy $E_{ii}^{S,M}$, which is shown in the Kataura plot (Fig. 4).

ω_{RBM} depends on the tube diameter as follows:[102]

$$\omega_{RBM} = \frac{227}{d_t}\sqrt{1 + C_{env}d_t^2}, \tag{2}$$

where C_{env} quantifies the effect of the environment on the RBM frequency.[103,104] Therefore, Eq. (2) can be used to obtain the diameter of a single nanotube from the observed ω_{RBM}, the diameter distribution of SWNTs in a sample, and also the influence of the environment on the vibration properties of the SWNTs. Most samples in the literature present $C_{env} = 0.056\,nm^{-2}$, although higher values have been obtained, like $C_{env} = 0.082\,nm^{-2}$ for SWNT attached to the surface of crystalline quartz.[105,106] It is common to find in the literature the expression $\omega_{RBM} = A/d_t + B$, with various values of the A and B constants, but they all fit into Eq. (2) with $C_{env} = 0.056\,nm^{-2}$, varying from paper to paper because the simpler linear dependency fails to describe samples with different diameters.[103,104]

The $E_{ii}^{S,M}$ depends on both the diameter and the chiral angle,[107,108] and they can be easily implemented with the following empirical formula:[79]

$$E_{ii}(p, d_t, \theta) = a\frac{p}{d_t}\left[1 + b\log\frac{c}{p/d_t}\right] + \beta_p \cos 3\theta/d_t^2, \tag{3}$$

where $p = 1$, 2, 3, 4, and 5 for E_{11}^S, E_{22}^S, E_{11}^M, E_{33}^S, and E_{44}^S, respectively. E_{ii}^j ($j = S$ or M) is the optical transition energy from the ith valence energy subband to the ith conduction energy subband measured from the energy gap for semiconductor (S) or metallic (M) SWNTs. Because of the 1D Van Hove singularity for the electronic density states, the joint-density of states becomes singular at the E_{ii}^j. Furthermore, because of the strong electron–hole attraction, the optical transition is mediated by an exciton, with a discrete exciton energy. Since the empirical formula is fitted to the experimental data, the E_{ii} corresponds to the exciton energy at room temperature.

By combining Eq. (2) with Eq. (3), we can build the experimental Kataura plot, like in Fig. 5, which enables all the RBM analysis described here; furthermore, we need the analysis of the environmental effects on the SWNT optical transitions.[104,109] The dielectric constants of the surrounding materials around a SWNT, such as surfactant, modify both ω_{RBM} and $E_{ii}^{S,M}$, which is known as the environmental effect for the exciton. The environmental conditions, including strain[110–113] and temperature[114] variations, can change the values of E_{ii} by a few tens of meV to a few hundreds of

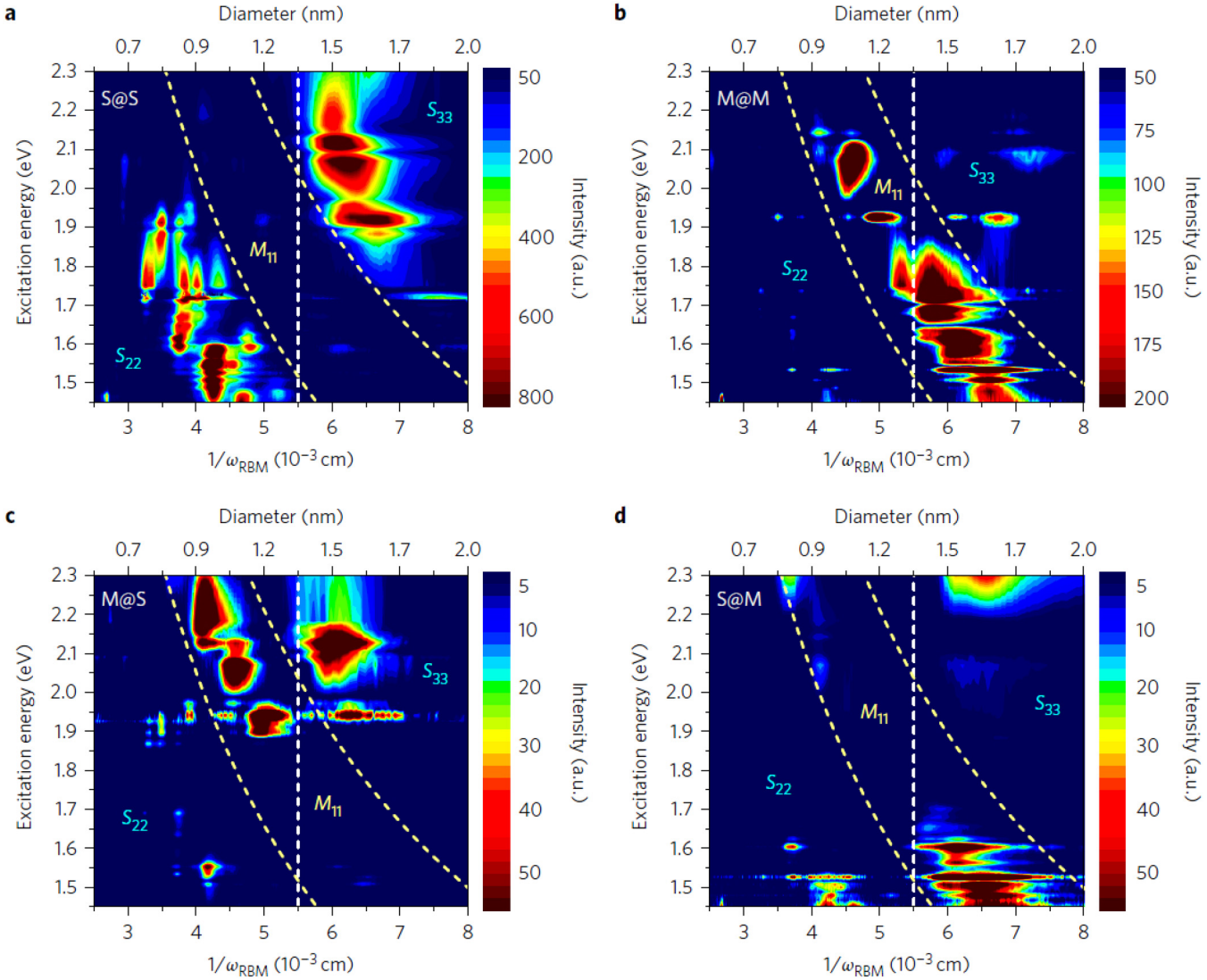

FIG. 6. RBM Raman intensity as a function of $1/\omega_{RBM}$ for (a) S@S, (b) M@M, (c) M@S, and (d) S@M DWNTs. The two curved dashed lines divide the energy ranges where the optical resonances of semiconducting (E_S^{22} or S_{22})–metallic (E_M^{11} or M_{11})–semiconducting (E_S^{33} or S_{33}) take place in SWNTs. Although the resonance energies and Raman cross sections vary from SWNTs to DWNTs, the overall trend does not change. To the right of the vertical dashed line appearing in the maps near $d_t = 1.3$ nm, the RBM signals come mostly from outer tubes (larger diameters), while to the left of this line, the RBM signals come mostly from inner tubes (small diameters). Reproduced with permission from Li *et al.*, Nat. Nanotechnol. **12**, 1176–1182 (2017). Copyright 2017 Springer Nature.

meV.[81,104,105,115,116] Therefore, when using Eq. (3) for one specific interest, the researcher may give some room for adjusting the fitting parameters. For an as-grown vertically aligned SWNT synthesized by the chemical vapor deposition method from alcohol, $a = 1.049$ eV nm, $b = 0.456$, and $c = 0.812$ nm^{-1} in Eq. (3) were found to properly fit the data.[79] A good review on the environmental effect can be found in Ref. 104.

For a quantitative analysis of the relative amount of the (n, m)'s in a sample from the RBM spectra, it is important to consider that the resonance Raman intensity depends on diameter and chiral angle. This problem has been addressed theoretically considering curvature and many-body effects, which are crucial for properly describing the optical phenomena.[117–120] Several experimental works were also performed to define these dependencies,[80,98,121] and for a simple-to-use empirical formula, we refer the reader to Ref. 80. It is important to note that one laser-excitation energy is not sufficient for evaluating the amount of (n, m)'s since only the resonant (n, m) SWNTs are observed in the Raman spectra, though we can only say that the resonant (n, m) SWNTs exist.

B. G and G′ (or 2D) bands for strain and doping characterization

Different from the RBM, which is observed only in SWNT, the G and G′ (also named 2D) bands are present in all sp^2 carbon structures. What makes these features special for applications is twofold: first, their high frequencies (the G band at $\sim 1584\,cm^{-1}$ and the G′ band at $\sim 2700\,cm^{-1}$) due to the small mass of the carbon atoms and a stiff C—C sigma bond. This is important because 0.1% variation in frequency represents already $1.5\,cm^{-1}$ for the G and $2.7\,cm^{-1}$ for the G′ bands, which are measurable shifts with most regular Raman spectrometers. First, a small change in the Raman shift or linewidths by ^{13}C isotope,[122] strain, or doping can be measured from the Raman spectra; second, because metallic sp^2 structures exhibit a strong electron–phonon coupling for a phonon, enabling detailed sensing of the Fermi level position via Raman spectroscopy. These two effects will be described here.

In Fig. 7(a), we show the G-band spectra for graphite (HOPG, top), semiconducting (middle), and metallic (bottom) SWNTs. Although the C—C bond stretching in graphene or graphite exhibits a single Lorentzian peak, SWNTs have two split peaks.[123] This happens because in the flat hexagonal lattice of graphite, the three C—C bond stretching vibration for a carbon atom is isotropic. However, when you impose a curvature in the sp^2 network to form a nanotube, symmetry breaking occurs by a curvature-induced strain in the direction perpendicular to the tube axis, which lowers the phonon frequency of the C—C vibrations which are preferentially in the circumferential direction.[123] On the other hand, the C—C vibrations in the direction parallel to the nanotube axis do not show the frequency shift. Thus, the curvature-induced frequency splitting between the higher and lower frequency components ($\omega_G^+ - \omega_G^-$) is inversely proportional to the square of the tube diameter and depends on the chiral angle [see Figs. 7(b) and 7(c)]. For example, the intensity ratio of G+ and G- depends on the chiral angle.[124] Some chiral angle dependence can also be found in small diameter SWNTs,[125] and a more strict analysis of the G-band line shape actually shows that this feature is composed by more than two peaks of different symmetries related to the confinement along SWNT circumference,[126–129] but two of these peaks (the totally symmetric) are predominant and for most application purposes the two-peaks analysis is simple and effective.[56]

The effect of strain[110,111] does not appear only due to curvature, but any tensile strain on a carbon nanotube or carbon nanotube fiber would shift the G and the G′ frequencies, in this case of the G band acting mainly on ω_G^+. Studies of uni-axial strain in graphene show both redshift and splitting of the G band are observed.[130–139] Studies on the effect in the G′ band can also be found in Ref. 140.

In the case of semiconductor SWNTs, ω_G^+ and ω_G^- correspond, respectively, to C—C bond stretching in the direction parallel (LO) and perpendicular (iTO) to the nanotube axis, when we consider the phonon propagating direction in the nanotube axis. However, in the case of metallic SWNTs, the assignment of ω_G^+ and ω_G^- becomes opposite [ω_G^+(iTO) and ω_G^-(LO)] to that for semiconductor nanotubes [see Fig. 7(c)].[56] This inversion happens because the LO mode becomes soft by the Kohn anomaly effect (electron–phonon coupling, see below and Secs. II and V A).

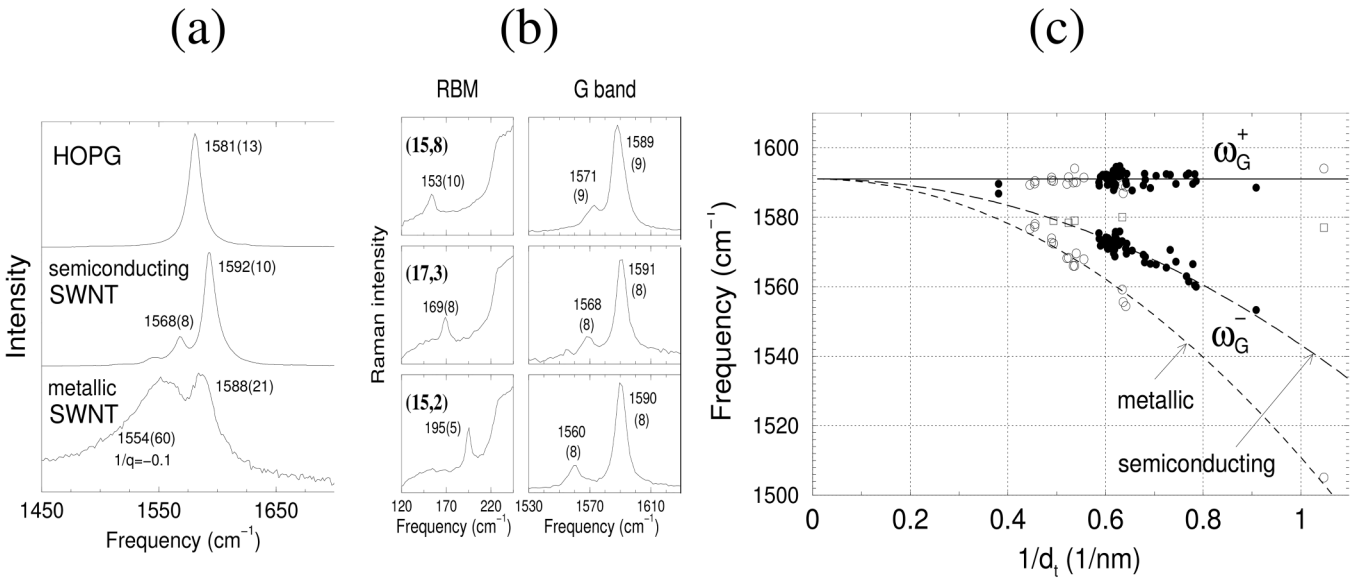

FIG. 7. (a) From top to bottom, G-band Raman spectra from HOPG, semiconducting, and a metallic SWNT bundles. Reproduced with permission from Dresselhaus *et al.*, Nano Lett. **10**, 751–758 (2010).[240] Copyright 2010 American Chemical Society. (b) RBM (left) and the G band (right) from isolated SWNTs dispersed on a silicon substrate. (c) ω_G^- and ω_G^+ for several isolated semiconducting (filled circles) and metallic (open circles) SWNTs, plotted as a function of $1/d_t$ extracted from the RBM frequency. The flat solid line shows $\omega_G^+ = 1591\,cm^{-1}$. The curves are given by the function $\omega_G^- = 1591 - C/d_t^2$, where $C = C_S = 47.7\,cm^{-1}\,nm^2$ for semiconducting SWNTs (long dashed curve) and $C = C_M = 79.5\,cm^{-1}\,nm^2$ for metallic SWNTs (short dashed curve). Also plotted (open squares) are the data for the $\sim 1580\,cm^{-1}$ Lorentzian peak sometimes observed in metallic SWNTs. Reproduced with permission from *Jorio et al.*, Phys. Rev. B **65**, 155412 (2002). Copyright 2002 American Physical Society.

As highlighted in Fig. 3(b), this electron–phonon coupling can be tuned by doping a gate electrode on a device, and the phonon-softening phenomenon of the G band is an evidence for metallic SWNT, as shown in Fig. 8. Therefore, the analysis of the G-band line shape of metallic SWNTs, as evidence in Fig. 8, can be used to monitor the Fermi level.[141,142] This effect will be further explored in Sec. V A, where the electro-chemical doping, which enables high doping levels will be addressed. It is noted that the Kohn anomaly effect is also predicted to occur for the RBM for metallic SWNTs, but the phonon softening effect is relatively small compared with that of the G band but chirality dependent.[76]

Notice that both strain and doping affect the frequencies and linewidths of the G and G′ bands. It has been demonstrated in graphene that a joint analysis of the G and G′ effects can separate each contribution of the two effects.[131,139,143] The picture is not so simple for a SWNT,[140] mostly because of the rich dependence of the G′ line shape on the electronic structure of specific (n, m) SWNTs. More specifically, the G′ frequency depends on the excitation laser energy (E_{laser} here in eV), by the following empirical formula (for SWNTs with $d_t \sim 1.5$ nm):[60]

$$\omega_{G'} = 2420 + 106E_{laser}, \quad (4)$$

as usually observed for other sp^2 carbons. This is an "average result" because the G′ frequency also depends on the tube diameter (see Sec. III C) and because, in SWNTs, the G′ is actually a multi-feature peak due to Raman processes with many phonon q vectors,

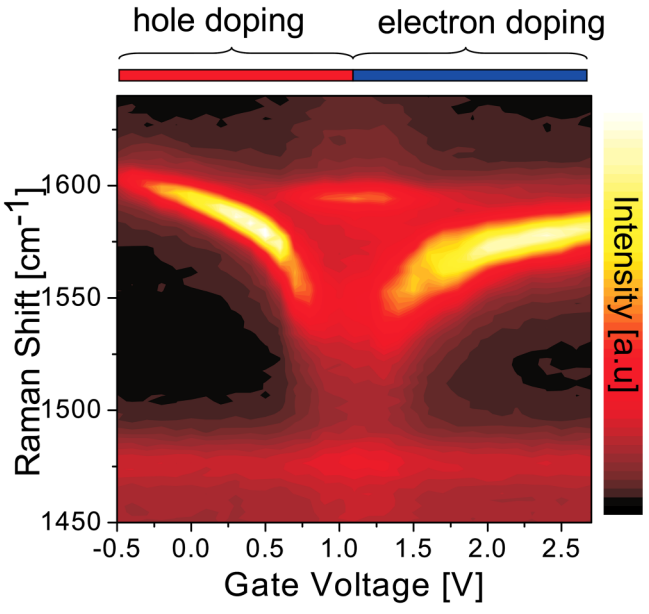

FIG. 8. Experimental intensity plot of the G-band spectrum of a metallic SWNT as a function of electrochemical gate potential. For this nanotube, the charge neutrality point, corresponding to the Dirac point, is at 1.2 V. Reproduced with permission from Farhat *et al.*, Phys. Rev. Lett. **99**, 145506 (2007). Copyright 2008 American Physical Society.

and the detailed line shape of the G′ band is dictated by resonances with (n, m) dependent optical transitions E_{ii}.[61,107,144,145] Therefore, when utilizing the G′ to characterize strain or doping, Eq. (4) can be utilized to extract the expected, averaged frequency of $\omega_{G'}$ as the starting point for the analysis. As already pointed, for large diameter tubes, like MWNTs, the learning from graphene ($d_t \to \infty$) applies more directly.

Another aspect related to the electron–phonon coupling is its effect on electronic devices, for example, limiting the current flowing in carbon nanotube transistors. Phonon population and electrical power dissipation can be quantified by simultaneously measuring the Stokes (phonon creating) and anti-Stokes (phonon annihilation) Raman scattering of the G mode (also of the radial-breathing mode) as a function of current bias.[146,147] The Stokes/anti-Stokes ratio is well established as a means to measure local temperature using Raman spectroscopy,[36] although a fine care must be taken with respect to the resonance conditions that is not the same for Stokes and anti-Stokes Raman spectra, as discussed in Refs. 148–151, or the presence of non-linear Stokes–anti-Stokes correlated generation, which has been observed in graphene[152–154] but not yet addressed in carbon nanotubes.

Since the Raman frequencies are sensitive to the mass of atoms, they can be used to identify isotope substitution. The G band in SWNTs shows a considerably redshift when replacing the ^{12}C atoms by ^{13}C.[155–157] Interestingly, Otsuka *et al.*[158] showed a method for tracing the diverse growth profiles of individual SWNTs by embedding digitally coded isotope labels, with potential not only to sensitively detect ^{13}C, but contributing also to further understanding and control of SWNT chirality, length, and density during synthesis.

C. D band for defect characterization

Defects in the nanotube structure change the properties of materials and generate interesting carbon nanotube-based structures.[65,159–161] Substitutional atoms, fictionalizing structures, formation of 7-5 ring pairs replacing hexagonal structures, dislocations, grain boundaries, and tube ends are all possible types of defects. The presence of defects in the sp^2 bond structure of graphene-related structures activates new Raman modes (see the three lower spectra in Fig. 1). The most prominent defect-induced peak is the so-called D band, appearing at $\sim$1350 cm^{-1}. Like the G′ band, the frequency of the D band depends on the excitation laser energy,[38,59–62] following an E_{laser} dependence like Eq. (4), but with the two constants having half of the values. A multi-peak structure[64,162] and an oscillatory dispersive behavior[163] have been observed for the D band in SWNT bundles (consistent with the observed G′ oscillatory dispersive behavior[60,164]). For isolated tubes, unusually sharp features can be seen in the D band with a full width half maximum (FWHM) intensity linewidth down to 7 cm^{-1}, owing to quantum confinement effects for the Raman process.[129] Furthermore, the D-band frequency also depends on the nanotube diameter (likewise for the overtone G′ band), with the following result for 514 nm (2.41 eV) laser excitation:[61,165]

$$\omega_D = 1354.8 - 16.5/d_t. \quad (5)$$

Together with Eqs. (4) and (5) provides the dependence of $\omega_{D,G'}$ on the fundamental aspects of the related Raman scattering in pristine SWNTs, and the deviations can be utilized as evidence for strain, doping, and other effects acting on a SWNT device.

The intensity of the D band is related to the amount of defects in the structure and broadly utilized to monitor the quality of graphene-related materials.[166–168] A single substitutional impurity in the wall of a SWNT can be visualized using the D-band imaging.[169] In particular, a well-defined substitutional B impurity in graphene gives a stronger and sharper D band than the G band.[170] Besides, broadening of the other peaks is also observed. For instance, Fig. 9 shows the Raman spectra of a carbon nanotube fiber at two locations: 1 is at the body of the fiber, where most nanotubes are pristine-like; 2 is at the very edge of the fiber, where the defective structure of the nanotube ends is prominent. The spectrum changes from a two-peaks sharp G-band feature without a D band at 1 to a broad and multi-peak G structure with a D band at 2.

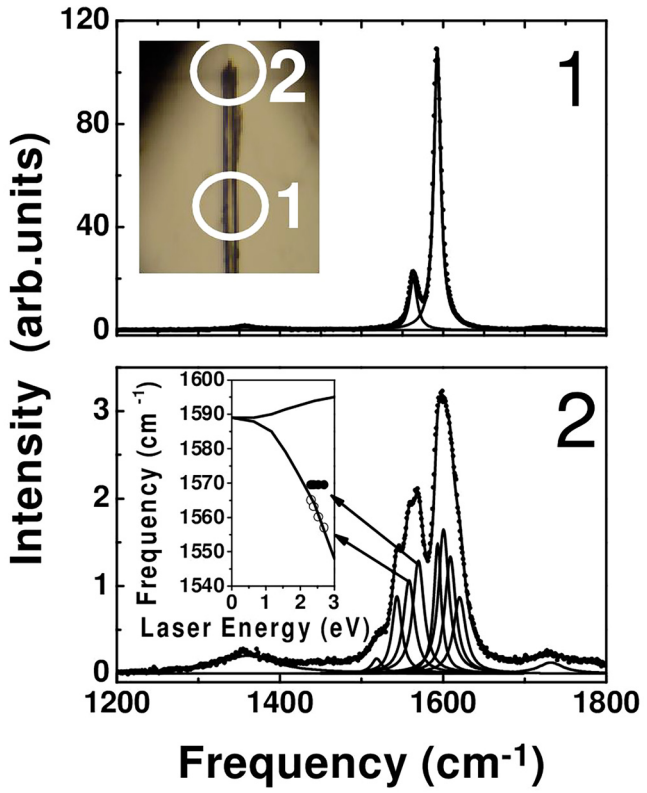

FIG. 9. G-band resonance Raman spectrum from a fiber of aligned SWNT bundles, with $E_{laser} = 2.71$ eV. The inset to the upper panel shows an optical image of the fiber. The spectrum in the upper panel was taken from location 1 (see the upper inset) with the incident and scattered light polarization aligned along the fiber axis. The spectrum in the lower panel was acquired from location 2 with the same polarization geometry. Reproduced with permission from Souza *et al.*, Phys. Rev. B **69**, R15424 (2004).[243] Copyright 2004 American Physical Society.

The intensity ratio between the G band and the disorder induced D band, I_D/I_G, has been a commonly used parameter for measuring the size L_a of a nano-crystal with ordered sp^2 C—C bonds or the amount of localized defects in the sp^2 network.[65,171–175] This defect-quantity metric has been extended to study the annealing effect on disordered multi-wall carbon nanotubes,[176] Si and C ion-implanted double-wall carbon nanotubes,[177] the effect of γ rays irradiated,[178] the boron and nitrogen doping levels in SWNTs[96,179] and MWNTs,[180] and to perform length characterization of DNA-wrapped carbon nanotubes.[181] Thus, the D-band intensity analysis relative to the G band is widely used for monitoring either the pristine quality or the intentional modifications (e.g., chemical functionalization) of CNTs for applications.

D. Final consideration and CNT composites

The concepts introduced in this section are basic and generally applicable to carbon nanotube-related materials. A class of materials that deserves attention are the carbon nanotube composites, where the carbon nanotubes are commonly utilized as a composite to change the properties of a host, such as polymers. Several authors addressed these materials, and the interested reader can find the Raman spectroscopy concepts discussed here utilized to characterize carbon nanotube composites in several articles, for example, in Refs. 46, 47, 49, 54, and 182. In this literature, Raman spectroscopy has been used not only to identify the carbon nanotubes within the composites, but also to access their dispersion, to evaluate nanotube/matrix interactions, and to detect polymer phase transitions.[49] Strain or stress transferred to nanotubes from the surrounding environment can be quantified both globally and locally, enabling the characterization of the elastic properties of the composite material, via Raman band frequency shifts, thus addressing the load transfer effectiveness among nanotubes and host.[46] For example, a G′ Raman band shift to a lower wavenumber upon application of a tensile stress indicates stress transfer from the matrix to the nanotubes and hence reinforcement by the nanotubes.[182] Furthermore, polarized Raman can be used to access the degree of carbon nanotube alignment, since the Raman signal is stronger when the light is polarized along the carbon nanotube axis.[44,127,128]

IV. RAMAN SPECTROSCOPY IMAGING OF SAMPLES AND DEVICES

One of the useful information by Raman spectroscopy is Raman imaging, in which the Raman intensity of a phonon mode is plotted as a function of the two-dimensional position (X,Y) of the sample or device surface. Three-dimensional imaging is also possible by adding a Z-scan, but much less usual since selectness and resolution are not efficient along the laser beam propagation direction, depending on the focusing geometry. Usually, the hyper spectra are obtained by raster scanning the laser in the sample/device, and acquiring one spectrum per (X,Y) point. The hyperspectral imaging is much more informative than simple microscopy imaging, because it carries all the spectral information at each point in the sample/device. In this section, we discuss how we can use Raman spectroscopy imaging for characterizing samples and the devices, addressing micro-Raman in Sec. IV A and

nano-Raman in Sec. IV B and presenting arguments in favor of Raman imaging by comparing it with the outcomes from other imaging techniques in Sec. IV C.

A. Micro-Raman spectroscopy imaging

A simple example of the use of micro-Raman spectroscopy imaging is when we put an isolated single-wall carbon nanotube on the SiO_2 surface and try to locate the SWNT at the specific position.[37] It is very hard to know the position of the nanotube on the surface since the diameter of SWNT is much smaller than the wavelength of the light, which means that it is not observable optically. Transmission electron microscope cannot be used for detecting the nanotube since the SiO_2 substrate is too thick to get the TEM images. By scanning the light focused by optical microscope over the device, we can get the Raman images with the spatial resolution in the order of half of the excitation wavelength ($\lambda/2$), generally in the 250–500 nm range. This technique is known as micro-Raman imaging in which we need to observe the Raman spectra at each spot of the light. Further, by using tip-enhanced Raman spectroscopy (TERS), the resolution becomes comparable to the nanotube diameter, in the nano-Raman imaging, as discussed in Sec. IV B.

As a more advanced example, Raman mapping of a SWNT serpentine (straight tube segments connected by U-turns, see Fig. 10)[183] shows how the Raman spectroscopy based image goes beyond the wavelength of light. The SWNT serpentine is deposited on non-isotropic quartz and their Raman spectrum depends on the tube–substrate morphology, which are shown in Fig. 10. The top part of the figure shows a micro-Raman G-band image with green pointers showing locations numbered from 1 (bottom right) to 41 (top left). A Raman spectrum was collected at each of those positions, and the G band is depicted in the color map shown in the bottom graphic, showing an oscillatory behavior of the G^+ peak near 1600 cm^{-1}, followed by the appearance and the disappearance of the broad metallic G^- signature around 1540 cm^{-1}. This means that the same SWNT-on-quartz system exhibits a mixture of semiconductor and metal behavior, depending on the orientation between the tube and the substrate. Therefore, Fig. 10 shows that different tube–substrate interactions for straight segments vs U-turns cause a modulation in the electronic properties along carbon nanotubes, forming an alternating semiconducting-metal-semiconducting-metal-· · ·nano-device.[106]

Another interesting device that has been proposed is the production of nanotube coil devices, including inductors, electromagnets, transformers, and dynamos. However, this type of construction commonly generates very defective nanotube coils. Nevertheless, such devices can be produced out of spontaneous self-coiling of the same SWNT into defect-free coils, going up to more than 70 turns with identical diameter and chirality, and these properties are corroborated by Raman imaging.[184,185] The left inset to panel (a) in Fig. 11 shows a Raman spectroscopy image of a SWNT coil formed by four complete turns. The image is based on the G-band Raman intensity [see device and characterization in panels (b)–(e)]. The black spectrum in (a) was taken at position 1 in the left inset, and the red spectrum at position 2 in the left inset. From the G-band line shape, the nanotube is identified to be semiconducting. The G-band signal in position 2 is significantly

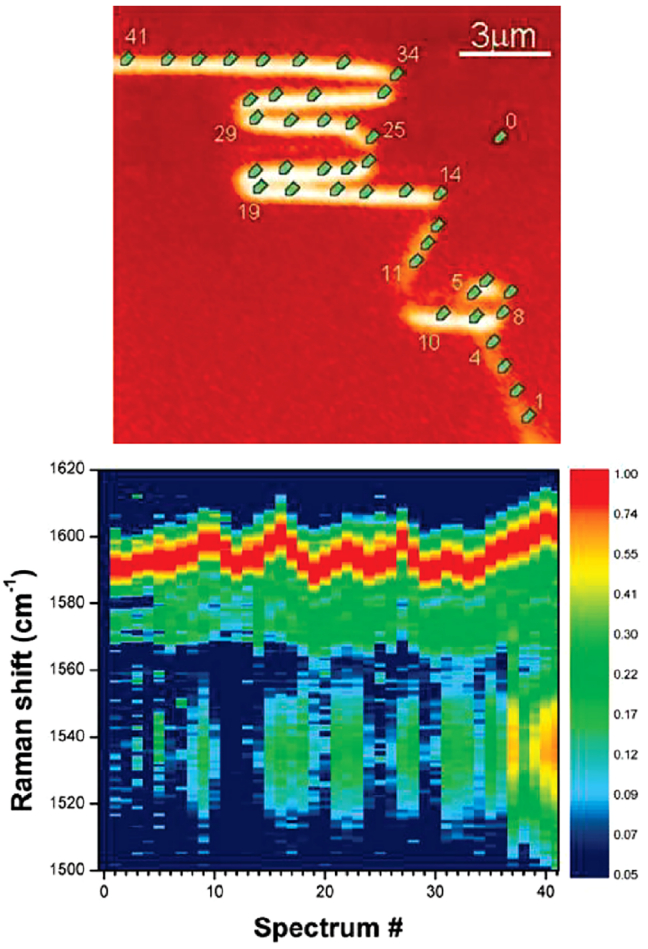

FIG. 10. Raman spectra along a SWNT serpentine on a quartz substrate. The substrate is miscut, thus forming atomic steps responsible for aligning the SWNTs during deposition. On the top, the confocal image of the G-band integrated intensity (E_{laser} = 1.96 eV, spatial resolution ~500 nm). At the bottom, the G-band Raman spectra obtained at the 41 points indicated by vertical green pointers and numbered in the upper panel. Reproduced with permission from Soares *et al.*, Nano Lett. **10**, 5043–5048 (2011). Copyright 2011 American Chemical Society.

stronger than in position 1 because the coil is composed of the signal of several nanotube turns. The D band is completely absent, demonstrating the structural integrity. The right inset is the low-frequency region of the spectrum, showing the RBM peak from the single-wall carbon nanotube at around 90 cm^{-1}, obtained from the free end segment, as well as the RBM overtone peak at ~180 cm^{-1}. The 90 cm^{-1} RBM is also present in the coil (position 2) but broadened by bundling.[184]

B. Nano-Raman spectroscopy imaging

While a regular microscope-based Raman system can be called a micro-Raman system, a tip-enhanced Raman spectroscopy

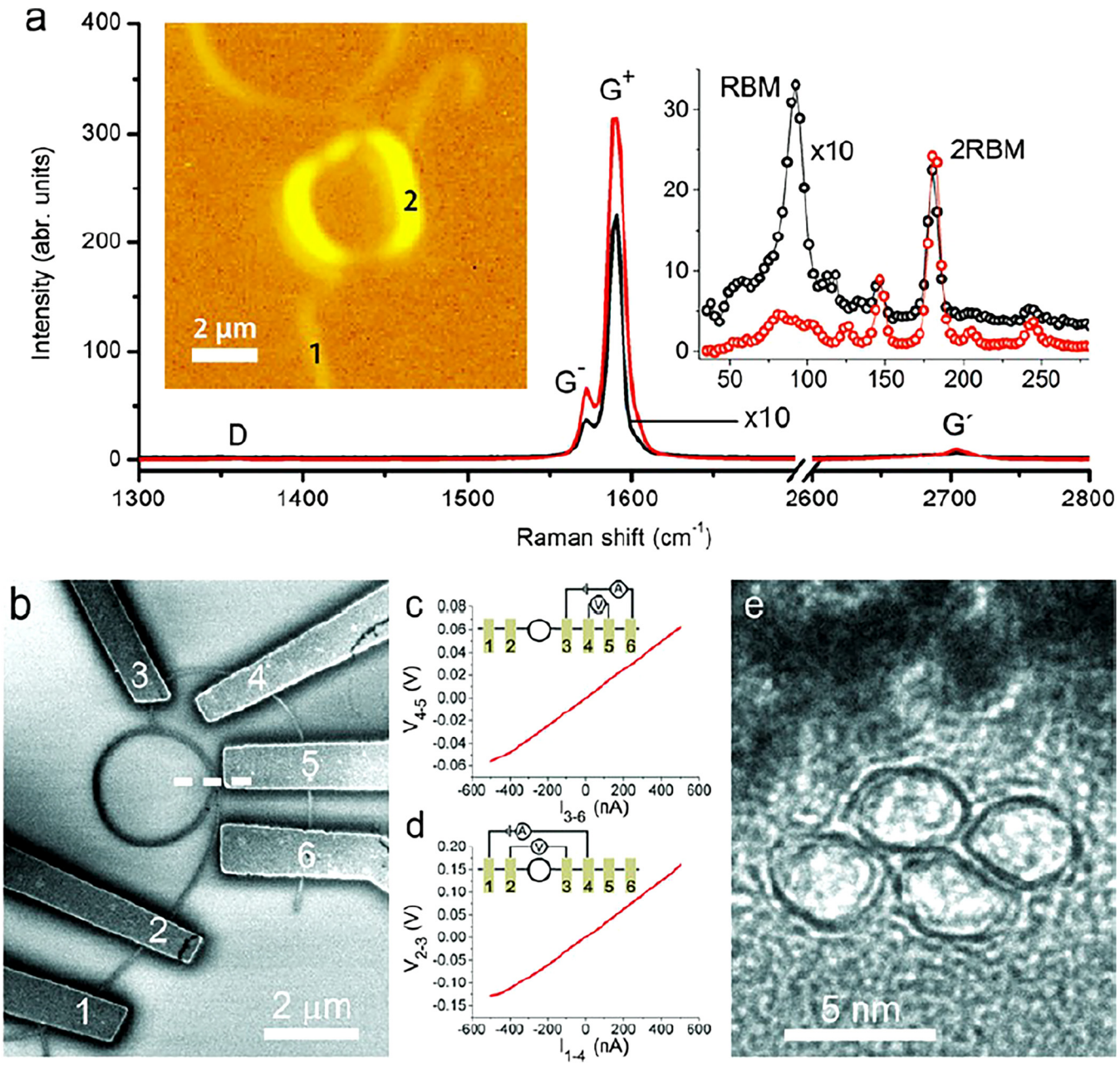

FIG. 11. (a) The left inset shows a G-band Raman spectral imaging of a SWNT coil utilized to build the device shown in (b)–(d). The main panel shows the G band as measured in positions 1 and 2 in the coil (see left inset), and the right inset shows the RBM spectra at these locations (black spectrum multiplied by 10). (b) An SEM image of the SWNT coil with Pd electrodes. [(c) and (d)] Four-point probe measurements on the free end and coil segments of the nanotube, respectively. (e) Cross-sectional TEM of the lamella taken at the position marked by a white dashed line in (b). Reproduced with permission from Shadmi *et al.*, Nano Lett. **16**, 2152–2158 (2016). Copyright 2016 American Chemical Society.

(TERS) system can be called a nano-Raman system. The nano-Raman system surpasses the resolution dictated by the light diffraction limit by scanning a plasmonic nano-antenna on the sample and extracting information from the near-field of light. Surface-enhanced Raman spectroscopy (SERS) is one of the most common techniques by using the spatially localized near-field. In fact, SERS has been applied to carbon nanotubes.[186–191] However, because of the sharp resonance Raman effect in the one-dimensional

structure, single-nanotube Raman spectroscopy by using the far-field can be achieved without any enhancement strategy of near-field.[37] Nevertheless, SWNTs became actually a prototype material for the advance of TERS, which is a variation of SERS where the plasmonic, local enhancement of the near-field is controlled by a scanning probe microscopy (SPM) system.[192,193] The merit of TERS is that TERS significantly improves the spatial resolution of Raman images. TERS provides a Raman imaging with a typical spatial resolution of ~10 nm, although resolution in the subnanometer scale has already been achieved.[194]

The comparison between micro-Raman and nano-Raman imaging is shown in Fig. 12. Panel (a) shows a micro-Raman image of the G band by scanning the laser spot over a carbon nanotube serpentine.[183] Panel (b) is an expanded image from the squared area in (a). Panel (c) is the nano-Raman image of the G band at the same location as (b), obtained by the nano-Raman (TERS). The blurred image in (b), which is actually defined by the size of the laser spot, is replaced by a sharp image in (c), which clearly resolves all details on the carbon nanotube serpentine.

In the nano-Raman spectroscopy, the strong near-field is generated on the surface of the nano-antenna by exciting surface plasmon.[195] The behavior of the near-field is shown by the "tip-approach curve" [see Fig. 12(f)], which describes the TERS intensity as a function of the tip-sample distance (Δ). The decaying nature of the near-field is well described with the classical electromagnetism theory by solving the Helmholtz equation for the electro-magnetic wave.[196–200] Except for tip-sample working distances below 1 nm, where quantum and atomistic effects on the plasmonic response have to be considered.[201] Nano-Raman in carbon nanotubes has been used to investigate local properties such as localized semiconductor-to-metal transition of a carbon nanotube[202] and electron and phonon renormalization near charged defects,[169] as shown in Fig. 13.

Figure 13 is an example of TERS for resolving local effects. It shows results from a (9,1) SWNT, where the Raman spectra in (a) were acquired at positions from R1 to R10 along the SWNT, as shown in (b), in steps of 10 nm. Figure 13(b) is a nano-Raman image based on the local intensity of the G band, and the yellow-dashed line is 100 nm in length, evidencing the high resolution of this Raman image. Notice in (a) a strong enhancement of the D peak at position R4, coincident with a localized photoluminescence (PL) emission shown in Fig. 13(c), indicating the presence of a defect acting as an exciton trapping state at R4. Analysis of the G′ peak (not shown in the figure) indicates that an exction trap state is formed by a negatively charged substitutional atom (nitrogen, in the case), which causes electron and phonon energies renormalization. Different TERS studies on

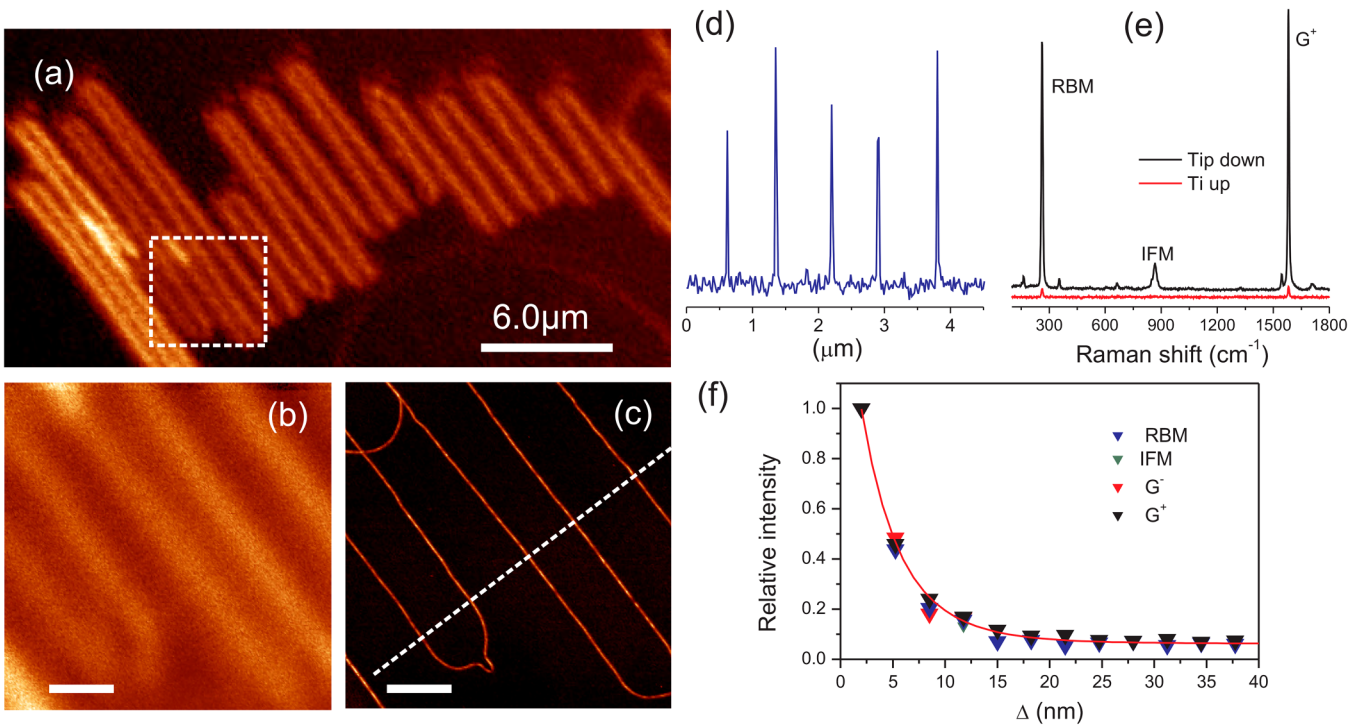

FIG. 12. (a) Confocal micro-Raman image of the G-band intensity in a serpentine of a semiconducting nanotube. The scale bar denotes 6 μm. (b) Expanded Raman image of the G-band intensity in the boxed area in panel (a). The scale bar corresponds to 800 nm. (c) Nano-Raman TERS image for the same region of (b). (d) G-band intensity along the white-dashed line in (c). (e) Far-field Raman spectrum (red or gray curve) and near-field Raman spectrum (black curve) recorded at the largest (~38 nm) and smallest (~2 nm) tip-sample separation, respectively. (e) Approach curves for the RBM, IFM, G^-, and G^+ bands. Reproduced with permission from Cançado *et al.*, Phys. Rev. Lett. **103**, 186101 (2009). Copyright 2009 American Physical Society.

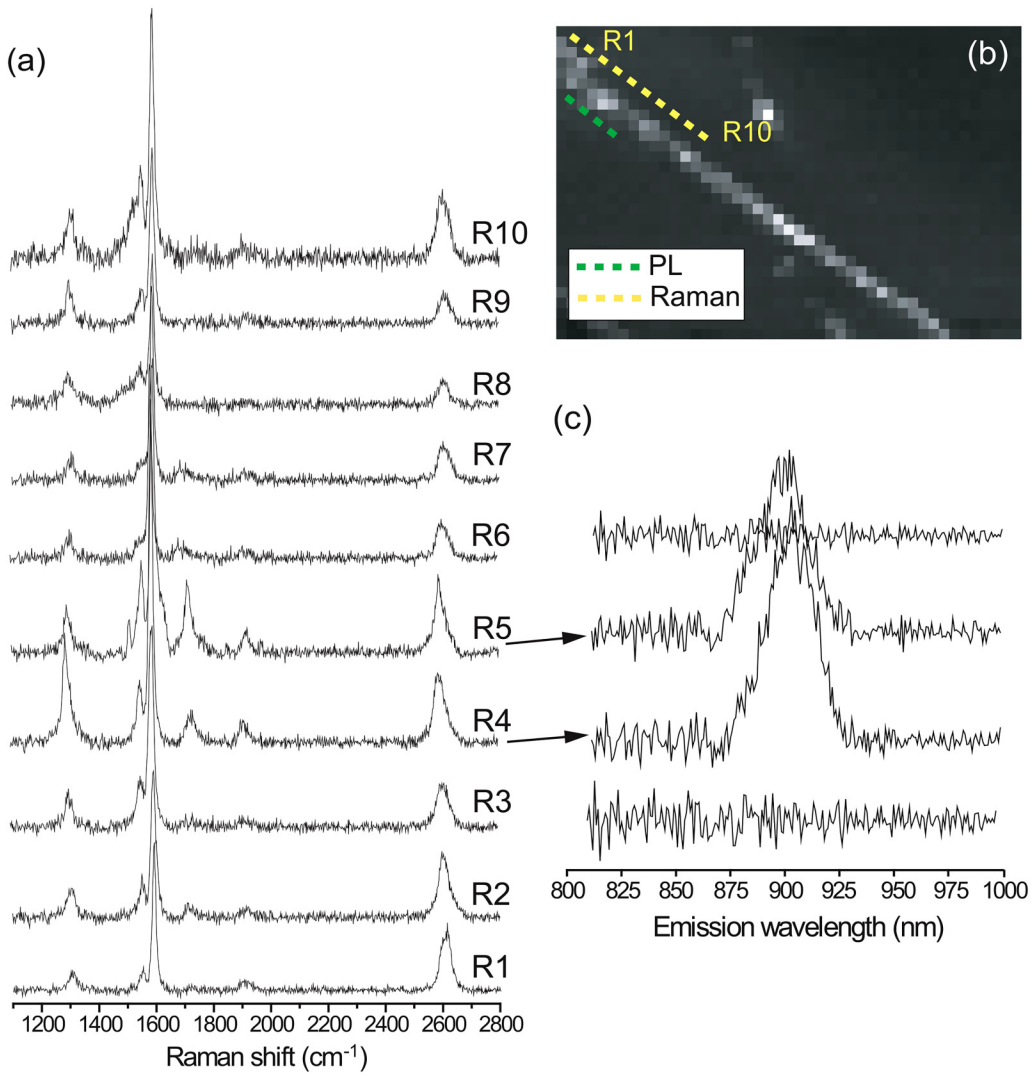

FIG. 13. Spectroscopic imaging of a (9,1) SWNT with $E_{laser} = 1.96$ eV (633 nm). (a) Local nano-Raman spectra obtained by moving the TERS tip along the R1–R10 yellow line in (b). (b) G-band spectral image of the SWNT, adapted with permission from Maciel *et al.*, Nat. Mater. **7**, 878–883 (2008). Copyright 2008 Springer Nature. (c) Photoluminescence emission at 904 nm along the green-dashed line in (b), corresponding to the same locations where the Raman spectra R3–R6 were taken.

SWNTs can be found in the literature,[192–195,202] including the presence of linear carbon chains inside carbon nanotubes.[203] A review of nano-Raman in carbon nanostructures, including carbon nanotubes, can be found in Ref. 204.

C. Comparison with other imaging techniques

Raman spectroscopy imaging is not yet integrated into industrial protocols, but we propose it should, based on the merits by comparing it with the existing methods. As already pointed out in Sec. I, RS has access to the fine electric and vibrational properties of the materials with a μeV energy resolution, superior to any other nanotechnology technique based on electron microscopy (e.g., electron energy-loss spectroscopy—EELS), scanning probe spectroscopies (SPSs), or even other optical techniques relying on less well-defined energy levels. Different optical techniques such as photoluminescence,[205–211] optical absorption,[212–214] and Rayleigh scattering[215–217] have provided a great contribution to the field of carbon nanotube characterization, including single nanotube (n, m) identification, but when going to functional information, such as doping and strain, they are not as sensitive in energy as looking at the phonon energies.

Raman imaging can be compared with XPS (x-ray photoelectron spectroscopy) or ESCA (Electron Spectroscopy for Chemical

Analysis) in which we can image the map of elements on the device or many other spectroscopies. Nowadays, the instrument that can measure several images at the same time is commercially available, which makes the characterization more precise and reliable information. Raman imaging has a lot of merits compared with other techniques. For example, Raman spectra can be observed in the ambient pressure while ESCA or TEM images requires the vacuum chamber. Further by changing the polarization direction of light in the polarized Raman spectroscopy, we can characterize the CNT alignment, the shape of the edge of graphene, strain direction, and other effects causing polarization selection. Raman imaging is also taken by applying the gate voltage on semiconductor devices, which can be directly compared with Kelvin force microscopy, in which the electro-static potential of the device as a function of the position is observed. In the Raman spectroscopy, the Kohn anomaly effect on the G band or RBM of carbon nanotubes can be observed as a function of the Fermi energy for each spot.

A further merit of Raman spectroscopy imaging is that, in principle, one can control the diameter of the incident light so that we first search the large area by a relatively large spot and then we focus on a specific region by much higher spatial resolution. Further, if we know the materials, we can focus on a narrow region of the Raman shift including the phonon frequency that we want to observe for saving time. Since the resonant Raman signal is sufficiently strong even for an isolated nanotube, we do not need to measure the Raman spectra for a long time if we just check if there are no signals on the specified point for several seconds.

Raman imaging can be used for characterizing (1) the edge structure, (2) the interface of the hetero-structure, (3) defects or impurity, (4) temperature gradient, (5) local strain, and (6) the Fermi energy. For (1)–(3), we frequently use the defect oriented Raman bands such as D and D′ bands[65,66] while for (4)–(6), the intrinsic Raman spectra such as the RBM, G, and G′ bands can be used. As for (4), it is known that the RBM frequency of nanotubes (or the G band of graphene) is monotonically decreased with increasing temperature for a wide region of temperature above the room temperature,[218] we can observe the temperature of the nanotube on the device as a function of the position. The local strain (5) is observed by the splitting of the G band and the Fermi energy is observed by the Kohn anomaly effect. In order to obtain these measurements, we do not need any further measurement but only micro-Raman setup.

V. COMPLEMENTARY ADVANCED TECHNIQUES

Having established the most well-understood and broadly utilized aspects of Raman spectroscopy to characterize carbon nanotubes for applications, we now introduce the fundamental aspects of some complementary advanced techniques with potential to help generating novel Raman spectroscopy-based applications, including electro-chemical doping (Sec. V A), circular dichroism (Sec. V B) and conservation of angular momentum (Sec. V C), and coherent phonon spectroscopy (Sec. V D). Here, we focus on those three examples, but we also briefly comment that there are other innovative and recent aspects in the field of Raman microscopy applied to CNT samples, for example: (i) CARS microscopy;[219] (ii) improved spatial resolution by structured illumination;[220] and (iii) the use of statistical spectrum processing methods to improve spectral analysis and the robustness of the information obtained,[221] among others that are not discussed here.

A. Electro-chemical doping

One of the fundamental techniques in semiconductor physics is doping of carriers in which the Fermi energy of the nanotubes and graphene-related materials is shifted from the Dirac point at the K points in the hexagonal Brillouin zone. In the field-effect transistor (FET), the carriers are doped in the channel region between the source and drain electrodes by applying the voltage at the gate electrode to enable electric current. When we apply the ionic gel in which the ion surrounded by a molecule is accumulated by the gate potential, we can change the Fermi energy more than 1 eV, which we call electro-chemical doping. In the electro-chemical doping, since we do not need insulator layers for the accumulated ions since the ions are surrounded by insulating molecules, the capacitance at the gate electrode becomes large, which is the reason for getting a large Fermi energy. A large change of the Fermi energy is useful for finding many physics such as superconducting phases and the Kohn anomaly effect though the speed of accumulation of charge in the gel is not so fast.

In electronic devices, it is important to evaluate the Fermi energy for a given gate voltage to obtain the carrier concentration or mobility. The Fermi energy is observed by many experimental methods such as scanning tunneling spectroscopy, the Hall conductivity, and angle-resolved photo-electron spectroscopy. Here, we show that non-contact Raman measurement can be used for evaluating the Fermi energy.

The Raman measurement by applying the gate voltage is called gate-modulated Raman spectroscopy,[222] in which the Fermi energy of graphene or nanotubes are given as a function of the gate voltage of either the top or the bottom gate. However, since the function depends on parameters of the gate electrode such as the area of electrodes, thickness, and dielectric constant of the dielectric materials as a capacitor, we cannot get a general form of the function. Thus, direct measurement of the Fermi energy is required for each device.

The spectral shape and frequency of the G band are sensitive to the Fermi energy, which is related to the Kohn anomaly effect. The Kohn anomaly effect is a phonon-softening effect in a metal as a perturbation for a phonon by electron–phonon interaction.[223] In Fig. 14, we show the illustration of the Kohn anomaly.[224] In the second-order perturbation for $q = 0$ phonon of the G band [Fig. 14(a)], the following two processes occur: (1) a phonon virtually excites a pair of electron (e) and hole (h) near the Fermi energy by electron–phonon interaction and (2) the excited pair recombines to emit a phonon. The phonon energy $\hbar\omega_{\mathbf{q}}$ with the wavevector $\mathbf{q}$ is modified by the electron–phonon interaction $V_{\mathbf{k}\mathbf{k}'}$ as follows:[225]

$$\hbar\omega_{\mathbf{q}} = \hbar\omega_{\mathbf{q}}^{(0)} + 2\sum_{\mathbf{k}\mathbf{k}'} \frac{|\mathrm{V}_{\mathbf{k}\mathbf{k}'}|^2}{\hbar\omega_{\mathbf{q}}^{(0)} - E^{\mathrm{eh}} + i\gamma_{\mathbf{q}}/2} \times (f_h - f_e), \tag{6}$$

where $\hbar\omega_{\mathbf{q}}^{(0)}$ is the unperturbed phonon energy and $E^{\mathrm{eh}} \equiv (E_{\mathbf{k}'}^{\mathrm{e}} - E_{\mathbf{k}}^{\mathrm{h}})$ represents the excitation energy for the e–h pair

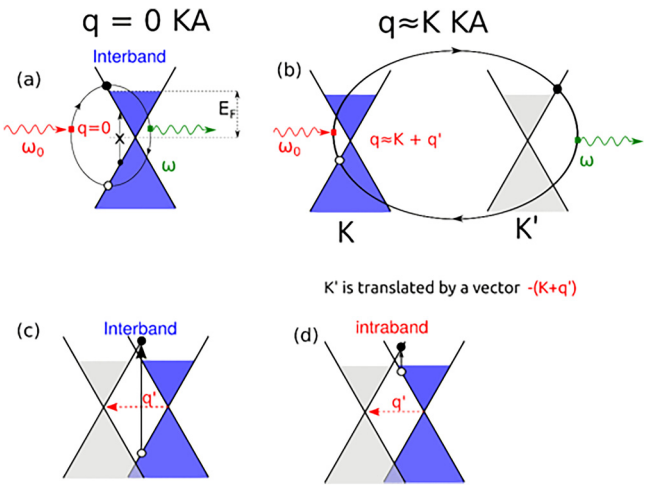

FIG. 14. (a) An illustration of the Kohn anomaly (KA) process for $\mathbf{q} = \mathbf{0}$ phonon, similar to Fig. 3(a). A phonon with zero wave vector ($\mathbf{q} = \mathbf{0}$) and frequency ω_0 vertically excites an electron–hole pair via the electron–phonon interaction. The electron–hole pair then recombines by emitting a phonon with frequency ω. (b) An illustration of KA for the $\mathbf{q} \sim$ K phonon. An electron exists at the K′ point leaving a hole behind at the K point with a distance in reciprocal space of $\mathbf{q} = \mathbf{K} + \mathbf{q}'$. If the K′ point is then translated by a vector $-(\mathbf{K} + \mathbf{q}')$, we can then imagine a virtual vertical transition of electron and hole. When $E_F \neq 0$, both interband (c) and intraband (d) transitions are expected. Reproduced with permission from Hasdeo *et al.*, Phys. Rev. B **94**, 075104 (2016). Copyright 2016 American Physical Society.

from the initial $\mathbf{k}$ to the final $\mathbf{k}'$ wavevector. In order to the momentum conservation, we get $\mathbf{q} \equiv \mathbf{k} - \mathbf{k}'$. $\gamma_\mathbf{q}$ is the energy uncertainty because of the finite lifetime of the e–h pair and $f_h(f_e)$ is the Fermi distribution function for a hole (an electron). Since $|V_{\mathbf{k}\mathbf{k}'}|^2$ and f_h–f_e are positive, the second term of Eq. (6) becomes negative (phonon softening) when the softening contribution for $\hbar\omega_\mathbf{q}^{(0)} - E^{\text{eh}} < 0$ in the summation on $\mathbf{k}, \mathbf{k}'$ is large compared with the hardening contribution for $\hbar\omega_\mathbf{q}^{(0)} - E^{\text{eh}} > 0$, which is the origin of the Kohn anomaly [see also Fig. 3(b)].

In the case of first-order Raman scattering, since the wavevector of the phonon is $\mathbf{q} = \mathbf{0}$, the excitation of the e–h pair occurs vertically in the k space ($\mathbf{k} = \mathbf{k}'$) near the K point in the Brillouin zone as shown in Fig. 14(a). When the Fermi energy, E_F is a positive (negative) value, the excitation with the E^{eh} up to $2E_\text{F}$ is suppressed because the final state is occupied (the initial state is unoccupied). When the E_F increases from zero to $\hbar\omega_\mathbf{q}^{(0)}/2$, the phonon frequency becomes soft since the hardening contribution is partially suppressed. When the E_F further increases more than $\hbar\omega_\mathbf{q}^{(0)}/2$, the phonon frequency becomes hard since the softening contribution is partially suppressed.

In Fig. 14(b), we show the Kohn anomaly for G′ phonon in which phonon $\mathbf{q}$ vector exists around the K point. In this case, the electron is excited from the K to K′ valleys leaving a hole behind at the K point. For a specific phonon frequency $\omega_\mathbf{q}$, the correction term of $\hbar\omega_\mathbf{q} - \hbar\omega_\mathbf{q}^{(0)} \equiv \Pi(\omega_\mathbf{q} E_F)$ is called the self-energy. The self-energy, $\Pi(\omega_\mathbf{q}, E_F)$, is a complex function of $\mathbf{q}$, in which the real part gives a shift of the phonon energy $\hbar\omega_\mathbf{q} - \hbar\omega_\mathbf{q}^{(0)}$, and the imaginary part gives the broadening of the spectra. Thus, γ_q in Eq. (6) can be calculated self-consistently by the self-energy. It is noted in Figs. 14(c) and 14(d) that both (c) intraband and (d) interband excitations of the e–h pair are possible for the Kohn anomaly of $\mathbf{q} = \mathbf{0}$ phonon. As for $\mathbf{q} = \mathbf{K}$ phonon, we can then imagine a virtual vertical transition of electron and hole by translating a vector $-(\mathbf{K} + \mathbf{q}')$ in Figs. 14(c) and 14(d).[224]

B. Circular dichroism of nanotubes

Circular dichroism (CD) is defined by the nonequivalent optical absorption for left-handed circularly polarized light (LCP) and right-handed circularly polarized light (RCP). Since a chiral nanotube does not have a mirror symmetry for a mirror parallel to the nanotube,[42] we expect CD for chiral nanotubes if we can separate the enantiomer of left-handed and right-handed chiral nanotubes. CD is a relevant property for application since it can be used to generate optically active devices, with potential application to information doubling by left- and right-handed circularly polarized light in the optical fibers as a single-photon emitter.[15,16] Although CD is not a Raman spectroscopy, the CD spectrum is an important characterization tool for characterizing the enantiomer (either left-handed or right-handed nanotube) purity of the nanotubes from application because of bio-compatibility in which only left-handed molecules appears in bio-materials. It is somewhat confusing to show here that though the left-handed and right-handed nanotubes for an enantiomer pair gives the opposite sign of CD, all left-handed nanotubes do not give the same sign as CD.

By using the gel sorting of carbon nanotubes, Wei *et al.* observed the CD spectra of separated nanotube in solution since the gel is a natural product with left handed and thus not only single chirality (n, m) but also enantiomer is separated.[226] It is noted that CD is observed for a chiral fullerene, such as C_{76}.

Since a photon of LCP (RCP) has an angular momentum $+\hbar$ $(-\hbar)$ in the propagation direction, optical absorption of SWNT occurs from the μ to $\mu + 1$ $(\mu - 1)$ cutting lines when the incident light propagates in the direction perpendicular to the nanotube axis. The cutting lines are defined by a set of one-dimensional Brillouin zones of a SWNT in the two-dimensional Brillouin zone of graphene.[33,227] It is noted that the Kataura plot in Figs. 4(b) and 5 is from the μ to the μ cutting lines ($E_{\mu\mu}$), which is optically allowed for linearly polarized light in the direction parallel to the nanotube axis.

The optical transition occurs by the conservation of angular momentum.[228] Since the final states for a given initial state at the μth cutting line are not the same for LCP and RCP, we expect that the optical absorption probabilities for LCP and RCP may not be the same. However, since we have a time-reversal symmetry in the electronic structure of carbon nanotubes, the optical absorption probability for LCP from μ to $\mu + 1$ near the K point becomes the same as the optical absorption probability for RCP from $-\mu$ to $-\mu - 1$ near the K′ point, which gives zero value of CD. This means that the conventional theory for CD does not work for a chiral carbon nanotube.

Sato *et al.* calculated CD spectra,[228] which is compared with the experimental results[226] as shown in Fig. 15. Sato *et al.* have

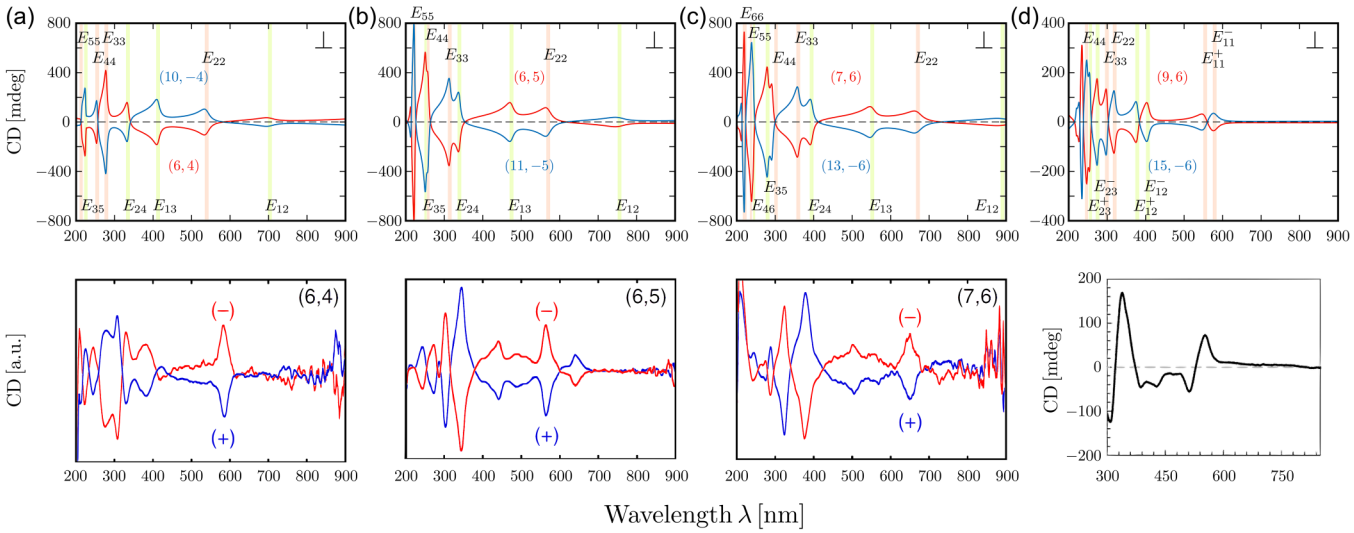

FIG. 15. In the top row, the calculated CD intensities of perpendicular [$CD^{\perp}(\lambda)$] case for (a) (6, 4) (red lines) and (10, − 4) (blue) type I s-SWNTs, (b) (6, 5) (red) and (11, − 5) (blue) type II s-SWNTs, (c) (7, 6) (red) and (13, − 6) (blue) type II s-SWNTs, and (d) (9, 6) (red) and (15, − 6) (blue) m-SWNTs. Van Hove singular transition energies at E_{ij} are shown in the vertically shaded area. Experimental data taken from Refs. 226 for s-SWNTs and 88 for m-SWNTs are shown at the bottom. The colors in the experiments do not correspond to the calculated results. As for (9,6) m-SWNT, only one CD spectrum is shown and the horizontal axis is from 300 to 750 cm^{-1}. Reproduced with permission from Sato *et al.*, Phys. Rev. B **95**, 155436 (2017). Copyright 2017 American Physical Society.

discussed the origin of the CD in a nanotube, in which the phase difference of the light at each carbon atom is essential for the appearance of CD.[228] The phase difference effect gives a shift of k vector in the optical transition in the direction of the K_2 (the direction of the cutting line), which breaks the symmetry of optical absorption probabilities between the K and K′ points for the light propagating in the direction parallel to the nanotube axis. As for the propagating direction perpendicular to the nanotube axis, the phase difference effect appears as a pre-factor (β) of the optical absorption.[228] By considering the enhancement of optical absorption by the exciton effect, the calculated CD values of undoped carbon nanotubes for the geometry of perpendicular incidence reproduce the experimentally observed CD spectra as a function of the wavelength as shown in Fig. 15.

Since the nanotube directions are random in the solution, we need to integrate CD values for the angle relative to the propagation direction of light. However, in the case of parallel incidence of light to the nanotube axis, since the depolarization effect[229] suppresses the electric field of LCP or RCP in the nanotube, we do not expect the CD values for this geometry. It is the reason why the calculated results of perpendicular incidence reproduce experimental results. The CD spectra for perpendicular incidence show the peak at E_{12}, E_{13}, E_{24}, E_{35}, and E_{46}, from the lower energy, which can be calculated by the calculation of the Kataura plot.[116,230]

By comparing with the peak positions of E_{ij}, we can assign the (n, m) indices of a nanotube. The enantiomer pair of (n, m) is $(n + m, -m)$, which gives an opposite sign of CD for (n, m), and thus we can assign $(n + m, -m)$ from the sign of CD. The sign of CD for E_{12} is given by the relative position of the nearest and second-nearest cutting lines near the K point. The relative position of the cutting lines is classified to be type-I and type-II semiconductor SWNTs, which are determined by the value of mod$(2n + m, 3)$=1 or 2, respectively[108,230] Thus, the sign of CD is opposite for type-I and type-II within the same handedness. Thus, the assignment of the enantiomer is uniquely determined by CD spectra by comparing the calculated results of E_{ij}.

C. Helicity-changing Raman spectra using circularly polarized light

When we use LCP for the incident light in the Raman spectroscopy, we observed the scattered RCP for a special Raman mode, which is called "helicity-changing Raman scattering." For example, the G band of graphene is a helicity-changing Raman mode.[231] The helicity-changing mode is assigned by calculating the Raman intensity, I

$$I \propto |{}^{t}P_s^{*} R P_i|^2, \tag{7}$$

where P_i, P_s, and R denote, respectively, the polarization vectors (or the Johns vectors) of the incident and scattered lights and the Raman tensor. Here, Ps for LCP and RCP that propagating in the direction of z are, respectively, given by

$$P_{\mathrm{LCP}} = \begin{pmatrix} 1 \\ i \\ 0 \end{pmatrix} \text{ and } P_{\mathrm{RCP}} = \begin{pmatrix} 1 \\ -i \\ 0 \end{pmatrix}. \tag{8}$$

When we adopt the Raman tensor of $E_{2g}(x^2 - y^2)$ for the G band, Eq. (7) has a non-zero value for the helicity-changing Raman

scattering as follows:

$$ {}^{t}P^{*}{}_{\mathrm{RCP}} R P_{\mathrm{LCP}} = (1, i, 0) \begin{pmatrix} e & 0 & 0 \\ 0 & -e & 0 \\ 0 & 0 & 0 \end{pmatrix} \begin{pmatrix} 1 \\ i \\ 0 \end{pmatrix} = 2e. \quad (9) $$

Since a photon of LCP (RCP) has a spin-angular momentum of $\hbar$ ($-\hbar$), in order to get the helicity-changing Raman scattering, we need a change of angular momentum by $2\hbar$ in a Raman scattering process. The angular momentum of an incident photon is transferred to the photo-excited electrons by electron–photon interaction.

The angular momentum of the electron is defined as follows. When the lattice has a n-fold rotation symmetry around the z axis, the Hamiltonian H is commutable with the rotational operator around the z axis with the angle $\alpha \equiv 2\pi/n$, $U(\alpha)$; that is, $[H, U(\alpha)] = 0$. In this case, any eigenfunction $|m>$ of H is also the eigenfunction of $U(\alpha)$; that is, $U(\alpha)|m>=C|m>$. Since U^n corresponding to 2π rotation, $C^n = 1$, which gives possible eigenvalues of $C = \exp(2\pi m i/n) = \exp(im\alpha)$, $(m = 0, 1, 2, \ldots, n-1)$. Here, we call m pseudo-angular momentum. In fact, the z component of the angular momentum, $L_z \equiv xp_y - yp_x$ is expressed as $L_z = -i\hbar\partial/\partial\varphi$ by spherical coordinate. The eigenfunction of L_z is given by $\exp(im\varphi)$, whose eigenvalue is $m\hbar$. If we multiply the $U(\alpha)$ to $\exp(im\varphi)$, we get

$$ U(\alpha)\exp(im\varphi) = \exp\{im(\varphi+\alpha)\} = \exp(im\alpha)\exp(im\varphi). \quad (10) $$

Equation (10) means that the eigenfunction of L_z, $\exp(im\varphi)$, is an eigenfunction of $U(\alpha)$ with an eigenvalue of $\exp(im\alpha)$. Thus, it is reasonable for us to call m a pseudo-angular momentum since the relationship is valid only for finite rotational angle α.

Since the electron–photon or electron–phonon matrix element is a scalar value that does not change by $U(\alpha)$, we can rotate the matrix element $\langle m'|O|m\rangle$ for any operator O, we get

$$ \langle m'|U^{-1}UOU^{-1}U|m\rangle = \exp i(m - m' + m_O)\alpha\langle m'|O|m\rangle, \quad (11) $$

where m_O represents the pseudo-angular momentum of the O defined by

$$ UOU^{-1} = \exp i(m_O)O. \quad (12) $$

In order to satisfy Eq. (12), U and O should be commutable. It is noted that O generally has a lower symmetry than H and that U should be selected for the lower rotational symmetry of O. If the matrix element has a N-fold rotational symmetry, the $\exp i(m - m' + m_O)$ should be the unity. Otherwise, by integration of the matrix element over the φ from 0 to 2π, the integration would give zero. From this fact, we get the conservation law of angualr momentum as follows:

$$ m - m' + m_O = Np, \quad (13) $$

where p is any integer. Equation (13) is understood by the conservation law of angular momentum.

Tatsumi *et al.* discussed the conservation of angular momentum in the Raman scattering process, which consists of two electron–photon and one electron–phonon matrix elements.[232] For the electron–photon matrix elements for circularly polarized light, $m_O = \sigma_i$ or σ_s where $\sigma_i = \pm 1$ or $\sigma_s = \pm 1$ denotes the helicity [or (spin-angular momentum)/$\hbar$] for the incident and scattered light, respectively. Since the photon of circularly polarized light has a rotational symmetry for any angles, the N in Eq. (13) becomes the rotational symmetry of the lattice. For the electron–phonon matrix element for the νth phonon mode, $m_O = m_\nu^{\mathrm{ph}}$, that is, the angular momentum of the phonon and N becomes the rotational symmetry of the νth phonon mode, N_ν.[232] Combining three equations for two electron–photon and one electron–phonon matrix elements in the first-order Raman process, we get the following rule of the conservation law of angular momentum for the first-order Raman process,

$$ \sigma_s - \sigma_i = -m_\nu^{\mathrm{ph}} + N_\nu p. \quad (14) $$

Helicity-changing Raman spectra are obtained when $\sigma_s - \sigma_i = \pm 2$.

In Table I, we list the symmetry of the phonon, ν, and the values of N, N_ν, m_ν^{ph}, and p that give the helicity-changing Raman spectra for the D_{2h}, D_{3h}, D_{4h}, and D_{6h} symmetries.[41,42] For example, the G band of graphene corresponds to the E_{2g} mode of D_{6h}. The in-plane Raman mode of TMDs corresponds to the E' mode of D_{3h}. From Table I, we can predict many unknown helicity-changing Raman signals for a twofold or fourfold rotational symmetry in Table I. Although the point group symmetry shows only D_{nh} in Table I, conservation law appears for both the higher and lower symmetries. For a lower symmetry, we can use Table I, too, since N_ν in the lower symmetry is either 1 or 2. For a higher symmetry such as T_d, and O_h, I_h, the angular momentum can be discussed for each high symmetry axis if the symmetry axis has a unique direction relative to the propagation direction of the light.

The helicity changing Raman spectra can assign the symmetry of the phonon, which is independent of characterization by polarized Raman spectra.[126,128,233] Thus, it will be useful for low-dimensional materials.

TABLE I. Conservation law of angular momentum in the helicity-changing Raman active modes in D_{2h}, D_{3h}, D_{4h}, and D_{6h} point groups.[41,42] We assume the direction of the light propagation along the z axis. Reproduced with permission from Tatsumi *et al.*, Phys. Rev. B 97, 195444 (2018). Copyright 2018 American Physical Society.

Symmetry	ν	N	N_ν	Degeneracy	m_ν^{ph}	p for helicity change
D_{2h}	A_g	2	2	Non-degenerate	0	±1
D_{2h}	B_{1g}	2	2	Non-degenerate	0	±1
D_{3h}	E'	3	1	Degenerate	0,±1	±1, ± 2, ± 3
D_{4h}	B_{1g}	4	2	Non-degenerate	0	±1
D_{4h}	B_{2g}	4	2	Non-degenerate	0	±1
D_{6h}	E_{2g}	6	2	Degenerate	0,±1	±1

D. Coherent phonon spectroscopy

When we irradiate a material with a single-pulsed laser light (or pump pulse) with a time width of several femtoseconds (fs), the valence electrons excite almost at the same time. The photo-excited electrons start to oscillate phonons at the same time by electron–phonon interaction. Such phonons are called coherent phonons (CPs) since the phonons oscillate with the same phase. Since the CP is a macroscopic oscillation of the materials, the transmission (or reflection) probability of light for the material oscillates as a function of time delay from the pump pulse with the frequency of the phonon as shown in Fig. 16(a).[234,235] In Fig. 16(a), the oscillations of the transmission (or reflection) probability $\Delta T/T$ are measured by irradiating the second pulse of a laser (probe pulse) with changing the time delay. By taking a Fourier transformation of $\Delta T/T$, we get CP spectra that have peaks at the phonon frequencies as shown in Fig. 16(b).

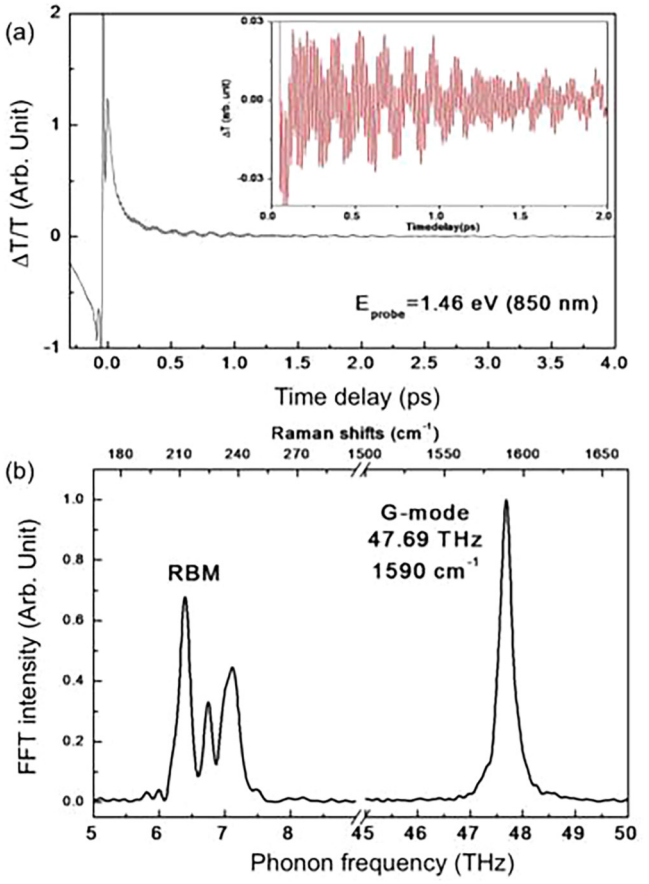

FIG. 16. Coherent phonon oscillations in single-walled carbon nanotubes and their fast Fourier transform power spectrum are shown. (a) Time-domain probe intensity modulations measured at 850 nm detection wavelength using a band-pass filter (BPF). The low-frequency oscillation with 160 fs is RBM mode, and tangential G mode emerges through the oscillation of 21 fs period. (b) Corresponding FFT spectrum in the frequency domain showing RBMs from 6.0*to*7.5 THz (200 ∼ 250 cm^{-1}) and G-mode at 47.69 THz (1590 cm^{-1}). Reproduced with permission from Kim *et al.*, Phys. Rev. B **86**, 161415 (2012). Copyright 2012 American Physical Society.

CP spectroscopy is similar to Raman spectroscopy since the CP spectra are given as a function of phonon frequency. CP spectroscopy requires a pump–probe measurement of laser optics, which is not easy for preparing the facility. Nevertheless, the CP method has many merits that Raman spectroscopy does not have. Let us list the unique points of CP: (1) CP spectra are free from the Rayleigh scattering; (2) the resonant condition is relaxed; (3) we can change the energy of the probe pulse; (3) we can change the repetition rate of the pumped pulse; (4) the initial phase of the phonon can be measured; and (5) the mixed sample of different SWNTs can be measured separately.

Since we do not measure the scattered light in CP, but the time modulation of transmission (or reflection) probability, the effect of Rayleigh scatting at the low frequency does not appear. In order to get the same phase of the oscillation of CP, the pulse width of the pump pulse should be much smaller than the period of the phonon oscillation, T. For example, since the period of the RBM modes at 100 cm^{-1} is 333 fs (T is given by $T = h/E$, where h is the Planck constant; 1 eV = 8065 cm^{-1} = 1.6×10^{-19} J), 50 fs is sufficient for pump pulse. However, the period of the oscillation for the G band (∼1600 cm^{-1}) is 20 fs, less than 10 fs is necessary to observe the G band by CP. For such a short pulse width, we know the uncertainty principles of quantum mechanics, $\Delta t \Delta E \geq \hbar$ in which ΔE for $\Delta t = T$ becomes 66 meV. The value of ΔE becomes large when we consider the short lifetime of the photo-excited electron. A large ΔE relaxes the resonant condition for the CP spectra, which makes many RBM peaks for a given laser energy.

One of the advantages of CP spectroscopy is that we can measure the CP signal of one (n, m) SWNT even in the mixed sample. In the case of Raman spectroscopy, we can measure the RBM of one (n, m) SWNT by using a sharp resonant effect by one-dimensional Van Hove singularity. However, in the case of CP, since the pump pulse is short, the resonant windows become large so that we cannot specify (n, m) by the resonant effect.

In CP spectroscopy, on the other hand, we use the so-called "pulse-train excitation," in which the incident pulses are injected repeatedly in the frequency of a RBM. When the repeated pulses generate CP for the specific (n, m) SWNT, the CP has the same phase as the phase of the repeated pulses, and thus the intensity of the CP becomes much larger than other CP intensities whose phases are random. In Fig. 17, we show the CP of pulse train excitation.[236,237] When we use a single pulse excitation as shown in Fig. 17(a), we show many beats in $\Delta T/T$ as a function of the time delay whose Fourier transform shows many peaks of RBM modes. When we set the repeated frequency of the incident pulses to 6.96 THz as shown in Fig. 17(b), we get only one peak of the RBM for (11,3) from the same mixed sample. Similarly by changing the repeated frequencies in Figs. 17(c) and 17(d), we get the corresponding CP peaks. This technique is useful for focusing the CP spectra in any mixed samples.

The pulse-train technique can be used for the G band. However, since the repeated frequency for the G band is much larger than that for RBM, no experiments adopt the technique for the G band. Nugraha *et al.* discussed the possibility of the pulse-

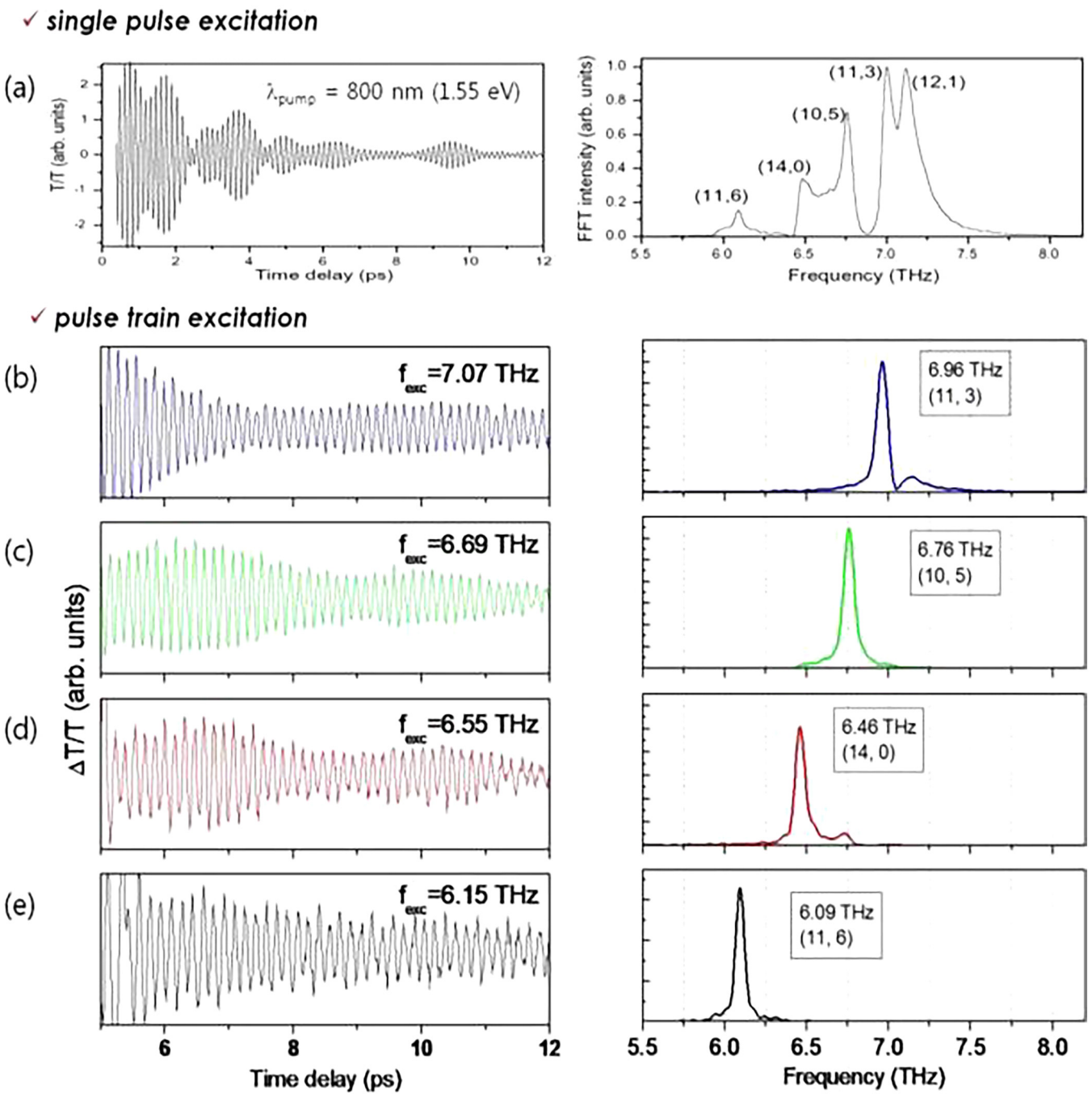

FIG. 17. (a) (Left) Time-domain transmission modulations of the probe due to coherent RBM vibrations in ensemble SWNT solution generated using standard pump–probe techniques without pulse shaping, (Right) Fourier transformation of time-domain oscillations with chirality assigned peaks. (b)–(e) (Left) Time-domain coherent RBM oscillations selectively excited by multiple pulse trains via pulse shaping with the corresponding repetition rates of 7.07 THz–6.15 THz; (Right) Fourier transformations of the corresponding oscillations, with their dominant nanotube chirality (*n*, *m*) indicated. Reproduced with permission from Kim *et al.*, Phys. Rev. Lett. **102**, 037402 (2009). Copyright 2009 American Physical Society.

train technique for the repeated pulse for several-integer times the period of the vibrational frequency.[238] It is also interesting to discuss the question of the RBM mode in CP spectra, whether the RBM mode starts by shrinking the diameter or by expanding the diameter. Since the initial force to a carbon atom by photo-excited electron is determined by the sign of electron–phonon interaction, the answer is that the direction depends on type-I or type-II SWNTs that has an opposite sign of electron–phonon interaction.[239] The initial phase of SWNT is measured by some experiments.

VI. CONCLUSIONS AND PERSPECTIVES

Raman spectroscopy in carbon nanotubes has been vastly studied in the last 20 years and it has reached the maturity to be utilized in applications. In this paper, we highlighted the use of Raman spectroscopy to help the development of applications based on carbon nanotubes, including several references from the literature, which runs from materials science to biotechnology. We focused initially on the well-established relations between the most prominent Raman features, namely, the RBM, D, G, and G′ bands, on carbon nanotube structure (diameter and helicity) and other external factors, such as strain, doping, the presence of defects, and environmental interactions. We provided equations, fitting parameters, and observed ranges of parameters that compose ready-to-use protocols. We then described how Raman spectroscopy has been used to characterize synthesis, selective sorting, doping, strain, and defects at the end of carbon fibers. Finally, we discussed micro- and nano-Raman imaging as a technique superior to standard microscopy, since spectroscopic imaging carries functional information, as well as other complementary advanced techniques that can be used to further improve the ability of Raman spectroscopy to characterize materials and devices.

A challenge to this field is the use of Raman spectroscopy not only as a method to characterize the materials and devices that will then be utilized independently of the Raman effect, but also using Raman response as the device working protocol itself. The carbon nanotubes can be designed as optical devices that will be read using Raman spectroscopy, and the Raman spectrum itself will be the functional indicator, for example, for sensors of strain, doping, and environmental conditions. The technique is mature for such an endeavor, while lasers and detectors are also becoming more powerful and cheaper, opening a route for novel disruptive innovations.

ACKNOWLEDGMENTS

A.J. and R.S. sincerely acknowledge the late Professor Mildred S. Dresselhaus, Professor Gene Dresselhaus, Professor Marcos A. Pimenta, and all collaborators for 20 years of collaboration on Raman spectroscopy. A.J. acknowledges CNPq (No. 302775/2018-8). R.S. acknowledges JSPS KAKENHI (No. JP18H01810).

DATA AVAILABILITY

The data that support the findings of this study are available from the corresponding author upon reasonable request.

REFERENCES

[1]Y.-P. Sun, K. Fu, Y. Lin, and W. Huang, "Functionalized carbon nanotubes: Properties and applications," Acc. Chem. Res. **35**, 1096–1104 (2002).
[2]V. N. Popov, "Carbon nanotubes: Properties and application," Mater. Sci. Eng. R **43**, 61–102 (2004).
[3]J. N. Coleman, U. Khan, W. J. Blau, and Y. K. Gun'ko, "Small but strong: A review of the mechanical properties of carbon nanotube–polymer composites," Carbon **44**, 1624–1652 (2006).
[4]M. Endo, M. S. Strano, and P. M. Ajayan, "Potential applications of carbon nanotubes," in *Carbon Nanotubes* (Springer, 2007), pp. 13–62.
[5]A. Jorio, M. S. Dresselhaus, and G. Dresselhaus, *Carbon Nanotubes: Advanced Topics in the Synthesis, Structure, Properties and Applications*, Topics in Applied Physics Vol. 111 (Springer-Verlag, Berlin, 2008), p. 720.
[6]P. J. Harris and P. J. F. Harris, *Carbon Nanotube Science: Synthesis, Properties and Applications* (Cambridge University Press, 2009).
[7]L. Hu, D. S. Hecht, and G. Gruner, "Carbon nanotube thin films: Fabrication, properties, and applications," Chem. Rev. **110**, 5790–5844 (2010).
[8]N. P. Guisinger and M. S. Arnold, "Beyond silicon: Carbon-based nanotechnology," MRS Bull. **35**, 273–279 (2010).
[9]M. S. Shaffer and A. H. Windle, "Fabrication and characterization of carbon nanotube/poly (vinyl alcohol) composites," Adv. Mater. **11**, 937–941 (1999).
[10]J. Li, C. Papadopoulos, J. Xu, and M. Moskovits, "Highly-ordered carbon nanotube arrays for electronics applications," Appl. Phys. Lett. **75**, 367–369 (1999).
[11]L.-M. Peng, Z. Zhang, and S. Wang, "Carbon nanotube electronics: Recent advances," Mater. Today **17**, 433–442 (2014).
[12]W. Hoenlein, F. Kreupl, G. S. Duesberg, A. P. Graham, M. Liebau, R. V. Seidel, and E. Unger, "Carbon nanotube applications in microelectronics," IEEE Trans. Compon. Packag. Technol. **27**, 629–634 (2004).
[13]N. De Jonge and J.-M. Bonard, "Carbon nanotube electron sources and applications," Philos. Trans. R. Soc. Lond. A **362**, 2239–2266 (2004).
[14]N. Lee, D. Chung, I. Han, J. Kang, Y. Choi, H. Kim, S. Park, Y. Jin, W. Yi, M. Yun *et al.*, "Application of carbon nanotubes to field emission displays," Diam. Relat. Mater. **10**, 265–270 (2001).
[15]X. Ma, N. F. Hartmann, J. K. Baldwin, S. K. Doorn, and H. Htoon, "Room-temperature single-photon generation from solitary dopants of carbon nanotubes," Nat. Nanotechnol. **10**, 671–675 (2015).
[16]X. He, H. Htoon, S. Doorn, W. Pernice, F. Pyatkov, R. Krupke, A. Jeantet, Y. Chassagneux, and C. Voisin, "Carbon nanotubes as emerging quantum-light sources," Nat. Mater. **17**, 663–670 (2018).
[17]R. Ramasubramaniam, J. Chen, and H. Liu, "Homogeneous carbon nanotube/polymer composites for electrical applications," Appl. Phys. Lett. **83**, 2928–2930 (2003).
[18]S. Park, M. Vosguerichian, and Z. Bao, "A review of fabrication and applications of carbon nanotube film-based flexible electronics," Nanoscale **5**, 1727–1752 (2013).
[19]D. N. Futaba, K. Hata, T. Yamada, T. Hiraoka, Y. Hayamizu, Y. Kakudate, O. Tanaike, H. Hatori, M. Yumura, and S. Iijima, "Shape-engineerable and highly densely packed single-walled carbon nanotubes and their application as super-capacitor electrodes," Nat. Mater. **5**, 987–994 (2006).
[20]D. Yu and L. Dai, "Self-assembled graphene/carbon nanotube hybrid films for supercapacitors," J. Phys. Chem. Lett. **1**, 467–470 (2010).
[21]Z. Fan, J. Yan, L. Zhi, Q. Zhang, T. Wei, J. Feng, M. Zhang, W. Qian, and F. Wei, "A three-dimensional carbon nanotube/graphene sandwich and its application as electrode in supercapacitors," Adv. Mater. **22**, 3723–3728 (2010).
[22]D. Zhang, K. Ryu, X. Liu, E. Polikarpov, J. Ly, M. E. Tompson, and C. Zhou, "Transparent, conductive, and flexible carbon nanotube films and their application in organic light-emitting diodes," Nano Lett. **6**, 1880–1886 (2006).
[23]D. D. Tune, B. S. Flavel, R. Krupke, and J. G. Shapter, "Carbon nanotube-silicon solar cells," Adv. Energy Mater. **2**, 1043–1055 (2012).
[24]A. Bianco, K. Kostarelos, C. D. Partidos, and M. Prato, "Biomedical applications of functionalised carbon nanotubes," Chem. Commun. **7**, 571–577 (2005).

[25]A. Jorio, *Bioengineering Applications of Carbon Nanostructures* (Springer, 2016).
[26]V. K. Upadhyayula, S. Deng, M. C. Mitchell, and G. B. Smith, "Application of carbon nanotube technology for removal of contaminants in drinking water: A review," Sci. Total Environ. **408**, 1–13 (2009).
[27]B. S. Harrison and A. Atala, "Carbon nanotube applications for tissue engineering," Biomaterials **28**, 344–353 (2007).
[28]Z. Liu, S. M. Tabakman, Z. Chen, and H. Dai, "Preparation of carbon nanotube bioconjugates for biomedical applications," Nat. Protoc. **4**, 1372–1381 (2009).
[29]P. W. Barone, S. Baik, D. A. Heller, and M. S. Strano, "Near-infrared optical sensors based on single-walled carbon nanotubes," Nat. Mater. **4**, 86–92 (2005).
[30]G. Gruner, "Carbon nanotube transistors for biosensing applications," Anal. Bioanal. Chem. **384**, 322–335 (2006).
[31]A. C. M. Dias, S. L. Gomes-Filho, M. M. Silva, and R. F. Dutra, "A sensor tip based on carbon nanotube-ink printed electrode for the dengue virus NS1 protein," Biosens. Bioelectron. **44**, 216–221 (2013).
[32]Z. Liu, W. Cai, L. He, N. Nakayama, K. Chen, X. Sun, X. Chen, and H. Dai, "In vivo biodistribution and highly efficient tumour targeting of carbon nanotubes in mice," Nat. Nanotechnol. **2**, 47–52 (2007).
[33]R. Saito, G. Dresselhaus, and M. S. Dresselhaus, *Physical Properties of Carbon Nanotubes* (Imperial College Press, London, 1998).
[34]D. Tománek, A. Jorio, M. S. Dresselhaus, and G. Dresselhaus, "Introduction to the important and exciting aspects of carbon-nanotube science and technology," in *Carbon Nanotubes* (Springer, 2007), pp. 1–12.
[35]S. Reich, C. Thomsen, and J. Maultzsch, *Carbon Nanotubes: Basic Concepts and Physical Properties* (John Wiley & Sons, 2008).
[36]A. Jorio, M. S. Dresselhaus, R. Saito, and G. Dresselhaus, *Raman Spectroscopy in Graphene Related Systems* (Wiley-VCH Verlag GmbH & Co KGaA, WeinHeim, 2010), p. 368.
[37]A. Jorio, R. Saito, J. H. Hafner, C. M. Lieber, M. Hunter, T. McClure, G. Dresselhaus, and M. S. Dresselhaus, "Structural (n, m) determination of isolated single-wall carbon nanotubes by resonant Raman scattering," Phys. Rev. Lett. **86**, 1118–1121 (2001).
[38]R. Saito, A. Jorio, A. G. Souza Filho, G. Dresselhaus, M. S. Dresselhaus, and M. A. Pimenta, "Probing phonon dispersion relations of graphite by double resonance Raman scattering," Phys. Rev. Lett. **88**, 027401 (2002).
[39]A. C. Ferrari, J. Meyer, V. Scardaci, C. Casiraghi, M. Lazzeri, F. Mauri, S. Piscanec, D. Jiang, K. Novoselov, S. Roth *et al.*, "Raman spectrum of graphene and graphene layers," Phys. Rev. Lett. **97**, 187401 (2006).
[40]Historically, the nomenclature using the letter "G" was utilized to identify the Raman peaks with the measured material, graphite. The G′ has been the dominant nomenclature until the work from Ferrari *et al.*, published in 2004, after what the graphene community adopted majorly the 2D nomenclature. It is important to recall, however, that the well-established nomenclature for a two-phonon overtone "2ω" considers two identical phonons (same ω and k) vibrating in phase as responsible for the light scattering. This is not the case for the G′ (or 2D) peak, where a collection of resonant ($\omega + \omega'$, $k + k'$) phonons without any phase correlation but respecting the internal resonance conditions (see the text) take place and, consequently, the G′ (or 2D, according to Ferrari *et al.*) peak is not an overtone of the D peak, and it does not appear at exactly twice the D peak frequency, this frequency difference ($\omega'_G \neq 2\omega_D$) depending on the excitation laser line.
[41]M. S. Dresselhaus, G. Dresselhaus, and A. Jorio, *Group Theory: Application to the Physics of Condensed Matter* (Springer, Berlin, 2008), p. 582.
[42]E. B. Barros, A. Jorio, G. G. Samsonidze, R. B. Capaz, A. G. Filho, J. M. Filho, G. Dresselhaus, and M. S. Dresselhaus, "Review on the symmetry related properties of carbon nanotubes," Phys. Rep. **431**, 261–302 (2006).
[43]H. Kataura, Y. Kumazawa, Y. Maniwa, I. Umezu, S. Suzuki, Y. Ohtsuka, and Y. Achiba, "Optical properties of single-wall carbon nanotubes," Synth. Met. **103**, 2555–2558 (1999).
[44]G. Duesberg, I. Loa, M. Burghard, K. Syassen, and S. Roth, "Polarized Raman spectroscopy on isolated single-wall carbon nanotubes," Phys. Rev. Lett. **85**, 5436 (2000).
[45]A. Rao, J. Chen, E. Richter, U. Schlecht, P. Eklund, R. Haddon, U. Venkateswaran, Y.-K. Kwon, and D. Tomanek, "Effect of van der Waals interactions on the Raman modes in single walled carbon nanotubes," Phys. Rev. Lett. **86**, 3895 (2001).
[46]V. Hadjiev, M. Iliev, S. Arepalli, P. Nikolaev, and B. Files, "Raman scattering test of single-wall carbon nanotube composites," Appl. Phys. Lett. **78**, 3193–3195 (2001).
[47]H. Kuzmany, R. Pfeiffer, M. Hulman, and C. Kramberger, "Raman spectroscopy of fullerenes and fullerene-nanotube composites," Philos. Trans. R. Soc. Lond. A **362**, 2375–2406 (2004).
[48]C. Thomsen, S. Reich, and J. Maultzsch, "Resonant Raman spectroscopy of nanotubes," Philos. Trans. R. Soc. Lond. A **362**, 2337–2359 (2004).
[49]Q. Zhao and H. D. Wagner, "Raman spectroscopy of carbon-nanotube-based composites," Philos. Trans. R. Soc. Lond. A **362**, 2407–2424 (2004).
[50]J. C. Meyer, M. Paillet, T. Michel, A. Moréac, A. Neumann, G. S. Duesberg, S. Roth, and J.-L. Sauvajol, "Raman modes of index-identified freestanding single-walled carbon nanotubes," Phys. Rev. Lett. **95**, 217401 (2005).
[51]T. Belin and F. Epron, "Characterization methods of carbon nanotubes: A review," Mater. Sci. Eng. B **119**, 105–118 (2005).
[52]R. Graupner, "Raman spectroscopy of covalently functionalized single-wall carbon nanotubes," J. Raman Spectrosc. **38**, 673–683 (2007).
[53]Z. Liu, C. Davis, W. Cai, L. He, X. Chen, and H. Dai, "Circulation and long-term fate of functionalized, biocompatible single-walled carbon nanotubes in mice probed by Raman spectroscopy," Proc. Natl. Acad. Sci. **105**, 1410–1415 (2008).
[54]L. Bokobza and J. Zhang, "Raman spectroscopic characterization of multiwall carbon nanotubes and of composites," Express Polym. Lett. **6**, 601–608 (2012).
[55]T. Schmid, L. Opilik, C. Blum, and R. Zenobi, "Nanoscale chemical imaging using tip-enhanced Raman spectroscopy: A critical review," Angew. Chem. Int. Ed. **52**, 5940–5954 (2013).
[56]A. Jorio, A. G. Souza Filho, G. Dresselhaus, M. S. Dresselhaus, A. K. Swan, M. S. Ünlü, B. Goldberg, M. A. Pimenta, J. H. Hafner, C. M. Lieber, and R. Saito, "G-band resonant Raman study of 62 isolated single wall carbon nanotubes," Phys. Rev. B **65**, 155412 (2002).
[57]C. Fantini, A. Jorio, M. Souza, L. O. Ladeira, M. A. Pimenta, A. G. Souza Filho, R. Saito, G. G. Samsonidze, G. Dresselhaus, and M. S. Dresselhaus, "One-dimensional character of combination modes in the resonance Raman scattering of carbon nanotubes," Phys. Rev. Lett. **93**, 087401 (2004).
[58]The Lorentzian shape is the typical resonant response of a damped harmonic oscillator with the external periodic forces. The central frequency at the Lorentzian peak corresponds to the eigen frequency of the oscillator while the spectral width of the Lorentzian is inversely proportional to the damping time.
[59]R. Saito, A. Grüneis, L. G. Cançado, M. A. Pimenta, A. Jorio, A. G. Souza Filho, M. S. Dresselhaus, and G. Dresselhaus, "Double resonance Raman spectra in disordered graphite and single wall carbon nanotubes," Mol. Cryst. Liq. Cryst. **387**, 63–72 (2002).
[60]M. A. Pimenta, E. B. Hanlon, A. Marucci, P. Corio, S. D. M. Brown, S. A. Empedocles, M. G. Bawendi, G. Dresselhaus, and M. S. Dresselhaus, "The anomalous dispersion of the disorder-induced and the second-order Raman bands in carbon nanotubes," Braz. J. Phys. **30**, 423–427 (2000).
[61]A. G. Souza Filho, A. Jorio, G. G. Samsonidze, G. Dresselhaus, M. A. Pimenta, M. S. Dresselhaus, A. K. Swan, M. S. Ünlü, B. B. Goldberg, and R. Saito, "Competing spring constant versus double resonance effects on the properties of dispersive modes in isolated single wall carbon nanotubes," Phys. Rev. B **67**, 035427 (2003).
[62]A. Grüneis, R. Saito, T. Kimura, L. G. Cançado, M. A. Pimenta, A. Jorio, A. G. Souza Filho, G. Dresselhaus, and M. S. Dresselhaus, "Determination of two-dimensional phonon dispersion relation of graphite by Raman spectroscopy," Phys. Rev. B **65**, 155405 (2002).
[63]First-order Raman scattering is the scattering of light by a single phonon. A second-order Raman scattering involves two phonons.
[64]J. Maultzsch, S. Reich, and C. Thomsen, "Chirality-selective Raman scattering of the D mode in carbon nanotubes," Phys. Rev. B **64**, 121407 (2001).

[65]M. A. Pimenta, G. Dresselhaus, M. S. Dresselhaus, L. G. Cançado, A. Jorio, and R. Saito, "Studying disorder in graphite-based systems by Raman spectroscopy," Phys. Chem. Chem. Phys. **9**, 1276–1291 (2007).
[66]R. Saito, A. Grüneis, G. G. Samsonidze, V. W. Brar, G. Dresselhaus, M. S. Dresselhaus, A. Jorio, L. G. Cançado, C. Fantini, M. A. Pimenta, and A. G. Souza Filho, "Double resonance Raman spectroscopy of single wall carbon nanotubes," New J. Phys. **5**, 157.1–157.15 (2003).
[67]C. Thomsen and S. Reich, "Double resonant Raman scattering in graphite," Phys. Rev. Lett. **85**, 5214 (2000).
[68]J. Kürti, V. Zólyomi, A. Grüneis, and H. Kuzmany, "Double resonant Raman phenomena enhanced by van Hove singularities in single-wall carbon nanotubes," Phys. Rev. B **65**, 165433 (2002).
[69]J. Maultzsch, S. Reich, and C. Thomsen, "Double-resonant Raman scattering in graphite: Interference effects, selection rules, and phonon dispersion," Phys. Rev. B **70**, 155403 (2004).
[70]S. Reich and C. Thomsen, "Raman spectroscopy of graphite," Philos. Trans. R. Soc. Lond. A **362**, 2271–2288 (2004).
[71]R. Saito, M. Hofmann, G. Dresselhaus, A. Jorio, and M. S. Dresselhaus, "Raman spectroscopy of graphene and carbon nanotubes," Adv. Phys. **60**, 413–550 (2011).
[72]A. C. Ferrari and D. M. Basko, "Raman spectroscopy as a versatile tool for studying the properties of graphene," Nat. Nanotechnol. **8**, 235–246 (2013).
[73]C. Fantini, A. Jorio, M. Souza, R. Saito, G. G. Samsonidze, M. S. Dresselhaus, and M. A. Pimenta, "Intermediate frequency Raman modes in metallic and semiconducting carbon nanotubes," in *Proceedings of the XVIII International Winter School on the Electronic Properties of Novel Materials*, edited by H. Kuzmany, J. Fink, M. Mehring, and S. Roth (American Institute of Physics, Woodbury, NY, 2005), Vol. 786, pp. 178–181.
[74]C. Fantini, A. Jorio, M. Souza, R. Saito, G. G. Samsonidze, M. S. Dresselhaus, and M. A. Pimenta, "Step-like dispersion of the intermediate frequent Raman modes in semiconducting and metallic carbon nanotubes," Phys. Rev. B **72**, 085446 (2005).
[75]S. D. M. Brown, A. Jorio, P. Corio, M. S. Dresselhaus, G. Dresselhaus, R. Saito, and K. Kneipp, "Origin of the Breit–Wigner–Fano lineshape of the tangential G-band feature of metallic carbon nanotubes," Phys. Rev. B **63**, 155414 (2001).
[76]K. Sasaki, R. Saito, G. Dresselhaus, M. S. Dresselhaus, H. Farhat, and J. Kong, "Chirality dependent frequency shift of radial breathing mode in metallic carbon nanotubes," Phys. Rev. B **78**, 235405 (2008).
[77]M. Machón, S. Reich, and C. Thomsen, "Strong electron-phonon coupling of the high-energy modes of carbon nanotubes," Phys. Rev. B **74**, 205423 (2006).
[78]M. J. O'Connell, S. Sivaram, and S. K. Doorn, "Near-infrared resonance Raman excitation profile studies of single-walled carbon nanotube intertube interactions: A direct comparison of bundled and individually dispersed HiPco nanotubes," Phys. Rev. B **69**, 235415 (2004).
[79]P. T. Araujo, S. K. Doorn, S. Kilina, S. Tretiak, E. Einarsson, S. Maruyama, H. Chacham, M. A. Pimenta, and A. Jorio, "Third and fourth optical transitions in semiconducting carbon nanotubes," Phys. Rev. Lett. **98**, 067401 (2007).
[80]P. B. C. Pesce, P. T. Araujo, P. Nikolaev, S. K. Doorn, K. Hata, R. Saito, M. S. Dresselhaus, and A. Jorio, "Calibrating the single-wall carbon nanotube resonance Raman intensity by high resolution transmission electron microscopy for a spectroscopy-based diameter distribution determination," Appl. Phys. Lett. **96**, 051910 (2010).
[81]P. Araujo, A. Jorio, M. S. Dresselhaus, K. Sato, and R. Saito, "Diameter dependence of the dielectric constant for the excitonic transition energy of single-wall carbon nanotubes," Phys. Rev. Lett. **103**, 146802 (2009).
[82]E. Joselevich, H. Dai, J. Liu, K. Hata, and A. H. Windle, "Carbon nanotube synthesis and organization," in *Carbon Nanotubes* (Springer, 2007), pp. 101–165.
[83]M. C. Hersam, "Progress towards monodisperse single-walled carbon nanotubes," Nat. Nanotechnol. **3**, 387–394 (2008).
[84]N. Komatsu and F. Wang, "A comprehensive review on separation methods and techniques for single-walled carbon nanotubes," Materials **3**, 3818–3844 (2010).
[85]D. Jariwala, V. K. Sangwan, L. J. Lauhon, T. J. Marks, and M. C. Hersam, "Carbon nanomaterials for electronics, optoelectronics, photovoltaics, and sensing," Chem. Soc. Rev. **42**, 2824–2860 (2013).
[86]J. A. Fagan, C. Y. Khripin, C. A. Silvera Batista, J. R. Simpson, E. H. Hároz, A. R. Hight Walker, and M. Zheng, "Isolation of specific small-diameter single-wall carbon nanotube species via aqueous two-phase extraction," Adv. Mater. **26**, 2800–2804 (2014).
[87]Y. Chen and J. Zhang, "Chemical vapor deposition growth of single-walled carbon nanotubes with controlled structures for nanodevice applications," Acc. Chem. Res. **47**, 2273–2281 (2014).
[88]G. Ao, J. K. Streit, J. A. Fagan, and M. Zheng, "Differentiating left- and right-handed carbon nanotubes by DNA," J. Am. Chem. Soc. **138**, 16677–16685 (2016).
[89]D. Janas, "Towards monochiral carbon nanotubes: A review of progress in the sorting of single-walled carbon nanotubes," Mater. Chem. Front. **2**, 36–63 (2018).
[90]H. Li, G. Gordeev, O. Garrity, N. A. Peyyety, P. B. Selvasundaram, S. Dehm, R. Krupke, S. Cambre, W. Wenseleers, S. Reich *et al.*, "Separation of specific single-enantiomer single-wall carbon nanotubes in the large-diameter regime," ACS Nano **14**, 948–963 (2019).
[91]M. Zheng, "Sorting carbon nanotubes," in *Single-Walled Carbon Nanotubes* (Springer, 2019), pp. 129–164.
[92]S. Zhang, L. Qian, Q. Zhao, Z. Wang, D. Lin, W. Liu, Y. Chen, and J. Zhang, "Carbon nanotube: Controlled synthesis determines its future," Sci. China Mater. **63**, 16–34 (2020).
[93]F. Yang, M. Wang, D. Zhang, J. Yang, M. Zheng, and Y. Li, "Chirality pure carbon nanotubes: Growth, sorting, and characterization," Chem. Rev. **120**, 2693–2758 (2020).
[94]C. Fantini, A. Jorio, A. Santos, V. Peressinotto, and M. Pimenta, "Characterization of dna-wrapped carbon nanotubes by resonance Raman and optical absorption spectroscopies," Chem. Phys. Lett. **439**, 138–142 (2007).
[95]C. Fantini, A. Jorio, M. Souza, M. S. Strano, M. S. Dresselhaus, and M. A. Pimenta, "Optical transition energies for carbon nanotubes from resonant Raman spectroscopy: Environment and temperature effects," Phys. Rev. Lett. **93**, 147406 (2004).
[96]I. Maciel, J. Campos-Delgado, E. Cruz-Silva, M. Pimenta, B. Sumpter, V. Meunier, F. López-Urías, E. Munoz-Sandoval, H. Terrones, M. Terrones *et al.*, "Synthesis, electronic structure, and Raman scattering of phosphorus-doped single-wall carbon nanotubes," Nano Lett. **9**, 2267–2272 (2009).
[97]A. Jorio, A. G. Souza Filho, G. Dresselhaus, M. S. Dresselhaus, A. Righi, F. M. Matinaga, M. S. S. Dantas, M. A. Pimenta, J. M. Filho, Z. M. Li, Z. K. Tang, and R. Saito, "Raman studies on 0.4 nm diameter single wall carbon nanotubes," Chem. Phys. Lett. **351**, 27–34 (2002).
[98]A. Jorio, A. P. Santos, H. B. Ribeiro, C. Fantini, M. Souza, J. P. M. Vieira, C. A. Furtado, J. Jiang, L. Balzano, D. E. Resasco, and M. A. Pimenta, "Quantifying carbon-nanotube species with resonance Raman scattering," Phys. Rev. B **72**, 075207 (2005).
[99]R. Pfeiffer, H. Kuzmany, C. Kramberger, C. Schaman, T. Pichler, H. Kataura, Y. Achiba, J. Kürti, and V. Zólyomi, "Unusual high degree of unperturbed environment in the interior of single-wall carbon nanotubes," Phys. Rev. Lett. **90**, 225501 (2003).
[100]R. Pfeiffer, F. Simon, H. Kuzmany, and V. Popov, "Fine structure of the radial breathing mode of double-wall carbon nanotubes," Phys. Rev. B **72**, 161404 (2005).
[101]H. Li, G. Gordeev, S. Wasserroth, V. S. K. Chakravadhanula, S. K. C. Neelakandhan, F. Hennrich, A. Jorio, S. Reich, R. Krupke, and B. S. Flavel, "Inner-and outer-wall sorting of double-walled carbon nanotubes," Nat. Nanotechnol. **12**, 1176–1182 (2017).
[102]P. T. Araujo, I. Maciel, P. Pesce, M. Pimenta, S. Doorn, H. Qian, A. Hartschuh, M. Steiner, L. Grigorian, K. Hata *et al.*, "Nature of the constant factor in the relation between radial breathing mode frequency and tube diameter for single-wall carbon nanotubes," Phys. Rev. B **77**, 241403 (2008).
[103]P. Araujo, C. Fantini, M. M. Lucchese, M. S. Dresselhaus, and A. Jorio, "The effect of environment on the radial breathing mode of supergrowth single wall carbon nanotubes," Appl. Phys. Lett. **95**, 261902 (2009).
[104]P. T. Araujo, P. B. C. Pesce, M. S. Dresselhaus, K. Sato, R. Saito, and A. Jorio, "Resonance Raman spectroscopy of the radial breathing modes in carbon nanotubes," Physica E **42**, 1251–1261 (2010).

[105]J. S. Soares, L. G. Cançado, E. B. Barros, and A. Jorio, "The Kataura plot for single wall carbon nanotubes on top of crystalline quartz," Phys. Status Solidi B **247**, 2835–2837 (2010).
[106]J. S. Soares, A. P. Barboza, P. T. Araujo, N. M. B. Neto, D. Nakabayashi, N. Shadmi, T. S. Yarden, A. Ismach, N. Geblinger, E. Joselevich, C. Vilani, L. G. Cançado, L. Novotny, G. Dresselhaus, M. S. Dresselhaus, B. R. Neves, M. S. Mazzoni, and A. Jorio, "Modulating the electronic properties along carbon nanotubes via tube-substrate interaction," Nano Lett. **10**, 5043–5048 (2011).
[107]G. G. Samsonidze, R. Saito, A. Jorio, A. G. Souza Filho, A. Grüneis, M. A. Pimenta, G. Dresselhaus, and M. S. Dresselhaus, "Phonon trigonal warping effect in graphite and carbon nanotubes," Phys. Rev. Lett. **90**, 027403 (2003).
[108]G. G. Samsonidze, R. Saito, N. Kobayashi, A. Grüneis, J. Jiang, A. Jorio, S. G. Chou, G. Dresselhaus, and M. S. Dresselhaus, "Family behavior of the optical transition energies in single-wall carbon nanotubes of smaller diameters," Appl. Phys. Lett. **85**, 5703–5705 (2004).
[109]Y. Miyauchi, R. Saito, K. Sato, Y. Ohno, S. Iwasaki, T. Mizutani, J. Jiang, and S. Maruyama, "Dependence of exciton transition energy of single-walled carbon nanotubes on surrounding dielectric materials," Chem. Phys. Lett. **442**, 394 (2007).
[110]S. Reich, H. Jantoljak, and C. Thomsen, "Shear strain in carbon nanotubes under hydrostatic pressure," Phys. Rev. B **61**, R13389 (2000).
[111]S. Reich, C. Thomsen, and P. Ordejon, "Elastic properties of carbon nanotubes under hydrostatic pressure," Phys. Rev. B **65**, 153407 (2002).
[112]R. B. Capaz, C. D. Spataru, P. Tangney, M. L. Cohen, and S. G. Louie, "Hydrostatic pressure effects on the structural and electronic properties of carbon nanotubes," Phys. Status Solidi B **241**, 3352–3359 (2004).
[113]S. Reich, C. Thomsen, and P. Ordejon, "Elastic properties and pressure-induced phase transitions of single-walled carbon nanotubes," Phys. Status Solidi B **235**, 354–359 (2003).
[114]S. Cronin, Y. Yin, A. Walsh, R. B. Capaz, A. Stolyarov, P. Tangney, M. L. Cohen, S. G. Louie, A. Swan, M. Ünlü *et al.*, "Temperature dependence of the optical transition energies of carbon nanotubes: The role of electron-phonon coupling and thermal expansion," Phys. Rev. Lett. **96**, 127403 (2006).
[115]P. Araujo, A. R. T. Nugraha, K. Sato, M. S. Dresselhaus, R. Saito, and A. Jorio, "Chirality dependence of the dielectric constant for the excitonic transition energy of single wall carbon nanotubes," Phys. Status Solidi B **247**, 2847–2850 (2010).
[116]A. R. T. Nugraha, R. Saito, K. Sato, P. T. Araujo, A. Jorio, and M. S. Dresselhaus, "Dielectric constant model for environmental effects on the exciton energies of single wall carbon nanotubes," Appl. Phys. Lett. **97**, 091905 (2010).
[117]J. Jiang, R. Saito, A. Grüneis, S. G. Chou, G. G. Samsonidze, A. Jorio, G. Dresselhaus, and M. S. Dresselhaus, "Intensity of the resonance Raman excitation spectra of single-wall carbon nanotubes," Phys. Rev. B **71**, 205420 (2005).
[118]J. Jiang, R. Saito, G. G. Samsonidze, S. G. Chou, A. Jorio, G. Dresselhaus, and M. S. Dresselhaus, "Electron-phonon matrix elements in single-wall carbon nanotubes," Phys. Rev. B **72**, 235408 (2005).
[119]J. Jiang, R. Saito, G. G. Samsonidze, A. Jorio, S. G. Chou, G. Dresselhaus, and M. S. Dresselhaus, "Chirality dependence of the exciton effects in single-wall carbon nanotubes," Phys. Rev. B **75**, 035407 (2007).
[120]J. Jiang, R. Saito, K. Sato, J. S. Park, G. G. Samsonidze, A. Jorio, G. Dresselhaus, and M. S. Dresselhaus, "Exciton-photon, exciton-phonon matrix elements and resonance Raman intensity," Phys. Rev. B **75**, 035405 (2007).
[121]A. Jorio, C. Fantini, M. A. Pimenta, D. A. Heller, M. S. Strano, M. S. Dresselhaus, Y. Oyama, J. Jiang, and R. Saito, "Carbon nanotube population analysis from Raman and photoluminescence intensities," Appl. Phys. Lett. **88**, 023109 (2006).
[122]S. D. Costa, C. Fantini, A. Righi, A. Bachmatiuk, M. H. Rmmeli, R. Saito, and M. A. Pimenta, "Resonant Raman spectroscopy on enriched 13C carbon nanotubes," Carbon **49**, 4719–4723 (2011).
[123]S. Reich, C. Thomsen, and P. Ordejón, "Phonon eigenvectors of chiral nanotubes," Phys. Rev. B **64**, 195416 (2001).
[124]R. Saito, A. Jorio, J. H. Hafner, C. M. Lieber, M. Hunter, T. McClure, G. Dresselhaus, and M. S. Dresselhaus, "Chirality-dependent G-band Raman intensity of carbon nanotubes," Phys. Rev. B **64**, 085312 (2001).
[125]H. Telg, J. G. Duque, M. Staiger, X. Tu, F. Hennrich, M. M. Kappes, M. Zheng, J. Maultzsch, C. Thomsen, and S. K. Doorn, "Chiral index dependence of the G+ and G- Raman modes in semiconducting carbon nanotubes," ACS Nano **6**, 904–911 (2012).
[126]A. M. Rao, A. Jorio, M. A. Pimenta, M. S. S. Dantas, R. Saito, G. Dresselhaus, and M. S. Dresselhaus, "Polarized Raman study of aligned multiwalled carbon nanotubes," Phys. Rev. Lett. **84**, 1820–1823 (2000), see also Comment in Phys. Rev. Lett. **85**, 3545 (2000).
[127]A. Jorio, A. G. Souza Filho, V. W. Brar, A. K. Swan, M. S. Ünlü, B. B. Goldberg, A. Righi, J. H. Hafner, C. M. Lieber, R. Saito, G. Dresselhaus, and M. S. Dresselhaus, "Polarized resonant Raman study of isolated single-wall carbon nanotubes: Symmetry selection rules, dipolar and multipolar antenna effects," Phys. Rev. B **65**, R121402 (2002).
[128]A. Jorio, M. A. Pimenta, A. G. Souza Filho, G. G. Samsonidze, A. K. Swan, M. S. Ünlü, B. B. Goldberg, R. Saito, G. Dresselhaus, and M. S. Dresselhaus, "Resonance Raman spectra of carbon nanotubes by cross-polarized light," Phys. Rev. Lett. **90**, 107403 (2003).
[129]A. Jorio, C. Fantini, M. S. S. Dantas, M. A. Pimenta, A. G. Souza Filho, G. G. Samsonidze, V. W. Brar, G. Dresselhaus, M. S. Dresselhaus, A. K. Swan, M. S. Ünlü, B. B. Goldberg, and R. Saito, "Linewidth of the Raman features of individual single-wall carbon nanotubes," Phys. Rev. B **66**, 115411 (2002).
[130]M. A. Bissett, W. Izumida, R. Saito, and H. Ago, "Effect of domain boundaries on the Raman spectra of mechanically strained graphene," ACS Nano **6**, 10229–10238 (2012.
[131]J. Zabel, R. R. Nair, A. Ott, T. Georgiou, A. K. Geim, K. S. Novoselov, and C. Casiraghi, "Raman spectroscopy of graphene and bilayer under biaxial strain: Bubbles and balloons," Nano Lett. **12**, 617–621 (2012).
[132]T. Yu, Z. Ni, C. Du, Y. You, Y. Wang, and Z. Shen, "Raman mapping investigation of graphene on transparent flexible substrate: The strain effect," J. Phys. Chem. C **112**, 12602–12605 (2008).
[133]D. Yoon, Y. W. Son, and H. Cheong, "Strain-dependent splitting of the double-resonance Raman scattering band in graphene," Phys. Rev. Lett. **106**, 155502 (2011).
[134]C. Si, Z. Sun, and F. Liu, "Strain engineering of graphene: A review," Nanoscale **8**, 3207–3217 (2016).
[135]Z. H. Ni, T. Yu, Y. H. Lu, Y. Y. Wang, Y. P. Feng, and Z. X. Shen, "Uniaxial strain on graphene: Raman spectroscopy study and band-gap opening," ACS Nano **2**, 2301–2305 (2008).
[136]T. Mohiuddin, A. Lombardo, R. Nair, A. Bonetti, G. Savini, R. Jalil, N. Bonini, D. Basko, C. Galiotis, N. Marzari *et al.*, "Uniaxial strain in graphene by Raman spectroscopy: G peak splitting, grüneisen parameters, and sample orientation," Phys. Rev. B **79**, 205433 (2009).
[137]W. Jie, Y. Yu Hui, Y. Zhang, S. Ping Lau, and J. Hao, "Effects of controllable biaxial strain on the Raman spectra of monolayer graphene prepared by chemical vapor deposition," Appl. Phys. Lett. **102**, 223112 (2013).
[138]M. Huang, H. Yan, T. F. Heinz, and J. Hone, "Probing strain-induced electronic structure change in graphene by Raman spectroscopy," Nano Lett. **10**, 4074–4079 (2010).
[139]C. Neumann, S. Reichardt, P. Venezuela, M. Drögeler, L. Banszerus, M. Schmitz, K. Watanabe, T. Taniguchi, F. Mauri, B. Beschoten *et al.*, "Raman spectroscopy as probe of nanometre-scale strain variations in graphene," Nat. Commun. **6**, 8429 (2015).
[140]M. Mohr, J. Maultzsch, and C. Thomsen, "Splitting of the Raman 2D band of graphene subjected to strain," Phys. Rev. B **82**, 201409 (2010).
[141]H. Farhat, H. Son, G. G. Samsonidze, S. Reich, M. S. Dresselhaus, and J. Kong, "Phonon softening in individual metallic carbon nanotubes due to the Kohn anomaly," Phys. Rev. Lett. **99**, 145506 (2007).
[142]K. Sasaki, R. Saito, G. Dresselhaus, M. S. Dresselhaus, H. Farhat, and J. Kong, "Curvature-induced optical phonon frequency shift in metallic carbon nanotubes," Phys. Rev. B **77**, 245441 (2008).

[143]J. E. Lee, G. Ahn, J. Shim, Y. S. Lee, and S. Ryu, "Optical separation of mechanical strain from charge doping in graphene," Nat. Commun. **3**, 1024 (2012).
[144]A. G. Souza Filho, A. Jorio, G. Dresselhaus, M. S. Dresselhaus, R. Saito, A. K. Swan, M. S. Ünlü, B. B. Goldberg, J. H. Hafner, C. M. Lieber, and M. A. Pimenta, "Effect of quantized electronic states on the dispersive Raman features in individual single wall carbon nanotubes," Phys. Rev. B **65**, 035404 (2002).
[145]A. G. Souza Filho, A. Jorio, A. K. Swan, M. S. Ünlü, B. B. Goldberg, R. Saito, J. H. Hafner, C. M. Lieber, M. A. Pimenta, G. Dresselhaus, and M. S. Dresselhaus, "Anomalous two-peak G'-band Raman effect in one isolated single-wall carbon nanotube," Phys. Rev. B **65**, 085417 (2002).
[146]M. Oron-Carl and R. Krupke, "Raman spectroscopic evidence for hot-phonon generation in electrically biased carbon nanotubes," Phys. Rev. Lett. **100**, 127401 (2008).
[147]M. Steiner, M. Freitag, V. Perebeinos, J. C. Tsang, J. P. Small, M. Kinoshita, D. Yuan, J. Liu, and P. Avouris, "Phonon populations and electrical power dissipation in carbon nanotube transistors," Nat. Nanotechnol. **4**, 320–324 (2009).
[148]A. G. Souza Filho, S. G. Chou, G. G. Samsonidze, G. Dresselhaus, M. S. Dresselhaus, L. An, J. Liu, A. K. Swan, M. S. Ünlü, B. B. Goldberg, A. Jorio, A. Grüneis, and R. Saito, "Stokes and anti-Stokes Raman spectra of small-diameter isolated carbon nanotubes," Phys. Rev. B **69**, 115428 (2004).
[149]A. G. Souza Filho, A. Jorio, J. H. Hafner, C. M. Lieber, R. Saito, M. A. Pimenta, G. Dresselhaus, and M. S. Dresselhaus, "Electronic transition energy E_ii for an isolated (n, m) single-wall carbon nanotube obtained by anti-Stokes/Stokes resonant Raman intensity ratio," Phys. Rev. B **63**, 241404R (2001).
[150]S. Doorn, D. Heller, P. Barone, M. Usrey, and M. Strano, "Resonant Raman excitation profiles of individually dispersed single walled carbon nanotubes in solution," Appl. Phys. A **78**, 1147–1155 (2004).
[151]G. Gordeev, A. Jorio, P. Kusch, B. G. Vieira, B. Flavel, R. Krupke, E. B. Barros, and S. Reich, "Resonant anti-stokes Raman scattering in single-walled carbon nanotubes," Phys. Rev. B **96**, 245415 (2017).
[152]A. Jorio, M. Kasperczyk, N. Clark, E. Neu, P. Maletinsky, A. Vijayaraghavan, and L. Novotny, "Optical-phonon resonances with saddle-point excitons in twisted-bilayer graphene," Nano Lett. **14**, 5687–5692 (2014).
[153]A. Jorio, M. Kasperczyk, N. Clark, E. Neu, P. Maletinsky, A. Vijayaraghavan, and L. Novotny, "Stokes and anti-stokes Raman spectra of the high-energy C–C stretching modes in graphene and diamond," Phys. Status Solidi B **252**, 2380–2384 (2015).
[154]C. A. Parra-Murillo, M. F. Santos, C. H. Monken, and A. Jorio, "Stokes–anti-stokes correlation in the inelastic scattering of light by matter and generalization of the Bose-Einstein population function," Phys. Rev. B **93**, 125141 (2016).
[155]S. Fan, L. Liu, and M. Liu, "Monitoring the growth of carbon nanotubes by carbon isotope labelling," Nanotechnology **14**, 1118 (2003).
[156]F. Simon, C. Kramberger, R. Pfeiffer, H. Kuzmany, V. Zólyomi, J. Kürti, P. Singer, and H. Alloul, "Isotope engineering of carbon nanotube systems," Phys. Rev. Lett. **95**, 017401 (2005).
[157]S. D. Costa, C. Fantini, A. Righi, A. Bachmatiuk, M. H. Rümmeli, R. Saito, and M. A. Pimenta, "Resonant Raman spectroscopy on enriched 13C carbon nanotubes," Carbon **49**, 4719–4723 (2011).
[158]K. Otsuka, S. Yamamoto, T. Inoue, B. Koyano, H. Ukai, R. Yoshikawa, R. Xiang, S. Chiashi, and S. Maruyama, "Digital isotope coding to trace the growth process of individual single-walled carbon nanotubes," ACS Nano **12**, 3994–4001 (2018).
[159]J.-C. Charlier, "Defects in carbon nanotubes," Acc. Chem. Res. **35**, 1063–1069 (2002).
[160]V. R. Coluci, D. S. Galvao, and A. Jorio, "Geometric and electronic structure of carbon nanotube networks: "Super"-carbon nanotubes," Nanotechnology **17**, 617 (2006).
[161]R. Lv, E. Cruz-Silva, and M. Terrones, "Building complex hybrid carbon architectures by covalent interconnections: Graphene-nanotube hybrids and more," ACS Nano **8**, 4061–4069 (2014).
[162]V. Zolyomi, J. Kürti, A. Grüneis, and H. Kuzmany, "Origin of the fine structure of the Raman D band in single-wall carbon nanotubes," Phys. Rev. Lett. **90**, 157401 (2003).
[163]S. D. M. Brown, A. Jorio, M. S. Dresselhaus, and G. Dresselhaus, "Observation of the D-band feature in the Raman spectra of carbon nanotubes," Phys. Rev. B **64**, 073403 (2001).
[164]A. G. Souza Filho, A. Jorio, G. Dresselhaus, M. S. Dresselhaus, R. Saito, A. K. Swan, M. S. Ünlü, B. B. Goldberg, J. H. Hafner, C. M. Lieber, and M. A. Pimenta, "Effect of quantized electronic states on the dispersive Raman features in individual single-wall carbon nanotubes," Phys. Rev. B **65**, 035404 (2001).
[165]M. A. Pimenta, A. Jorio, S. D. M. Brown, A. G. Souza Filho, G. Dresselhaus, J. H. Hafner, C. M. Lieber, R. Saito, and M. S. Dresselhaus, "Diameter dependence of the Raman D-band in isolated single-wall carbon nanotubes," Phys. Rev. B **64**, 041401 (2001).
[166]S. Arepalli, P. Nikolaev, O. Gorelik, V. G. Hadjiev, W. Holmes, B. Files, and L. Yowell, "Protocol for the characterization of single-wall carbon nanotube material quality," Carbon **42**, 1783–1791 (2004).
[167]Y. Li, X. Zhang, X. Tao, J. Xu, W. Huang, J. Luo, Z. Luo, T. Li, F. Liu, Y. Bao *et al.*, "Mass production of high-quality multi-walled carbon nanotube bundles on a Ni/Mo/Mgo catalyst," Carbon **43**, 295–301 (2005).
[168]J.-M. Feng, R. Wang, Y.-L. Li, X.-H. Zhong, L. Cui, Q.-J. Guo, and F. Hou, "One-step fabrication of high quality double-walled carbon nanotube thin films by a chemical vapor deposition process," Carbon **48**, 3817–3824 (2010).
[169]I. O. Maciel, N. Anderson, M. A. Pimenta, A. Hartschuh, H. Qian, M. Terrones, H. Terrones, J. Campos-Delgado, A. M. Rao, L. Novotny *et al.*, "Electron and phonon renormalization near charged defects in carbon nanotubes," Nat. Mater. **7**, 878–883 (2008).
[170]Y. A. Kim, K. Fujisawa, H. Muramatsu, T. Hayashi, M. Endo, T. Fujimori, K. Kaneko, M. Terrones, J. Behrends, A. Eckmann, C. Casiraghi, K. S. Novoselov, R. Saito, and M. S. Dresselhaus, "Raman spectroscopy of boron-doped single-layer graphene," ACS Nano **6**, 6293–6300 (2012).
[171]K. Sato, R. Saito, Y. Oyama, J. Jiang, L. G. Cançado, M. A. Pimenta, A. Jorio, G. G. Samsonidze, G. Dresselhaus, and M. S. Dresselhaus, "D-band Raman intensity of graphitic materials as a function of laser energy and crystallite size," Chem. Phys. Lett. **427**, 117–121 (2006).
[172]M. S. Dresselhaus, A. Jorio, A. G. Souza Filho, and R. Saito, "Defect characterization in graphene and carbon nanotubes using Raman spectroscopy," Philos. Trans. R. Soc. A **368**, 5355–5377 (2010).
[173]M. M. Lucchese, F. Stavale, E. M. Ferreira, C. Vilani, M. V. D. O. Moutinho, R. B. Capaz, C. A. Achete, and A. Jorio, "Quantifying ion-induced defects and Raman relaxation length in graphene," Carbon **48**, 1592–1597 (2010).
[174]L. G. Cançado, A. Jorio, E. M. Ferreira, F. Stavale, C. A. Achete, R. B. Capaz, M. V. D. O. Moutinho, A. Lombardo, T. Kulmala, and A. C. Ferrari, "Quantifying defects in graphene via Raman spectroscopy at different excitation energies," Nano. Lett. **11**, 3190–3196 (2011).
[175]L. G. Cançado, M. G. Da Silva, E. H. M. Ferreira, F. Hof, K. Kampioti, K. Huang, A. Pénicaud, C. A. Achete, R. B. Capaz, and A. Jorio, "Disentangling contributions of point and line defects in the Raman spectra of graphene-related materials," 2D Mater. **4**, 025039 (2017).
[176]Y. A. Kim, T. Hayashi, K. Osawa, M. S. Dresselhaus, and M. Endo, "Annealing effect on disordered multi-wall carbon nanotubes," Chem. Phys. Lett. **380**, 319–324 (2003).
[177]G. D. Saraiva, A. G. Souza Filho, G. Braunstein, E. B. Barros, J. Mendes Filho, E. Moreira, S. B. Fagan, D. L. Batista, Y. A. Kim, H. Muramatsu, M. Endo, and M. S. Dresselhaus, "Resonant Raman spectroscopy in Si and C ion-implanted double wall carbon nanotubes," Phys. Rev. B **80**, 155452 (2009).
[178]M. Hulman, V. Skákalová, S. Roth, and H. Kuzmany, "Raman spectroscopy of single-wall carbon nanotubes and graphite irradiated by γ rays," J. Appl. Phys. **98**, 024311 (2005).
[179]I. Maciel, J. Campos-Delgado, M. Pimenta, M. Terrones, H. Terrones, A. Rao, and A. Jorio, "Boron, nitrogen and phosphorous substitutionally doped single-wall carbon nanotubes studied by resonance Raman spectroscopy," Phys. Status Solidi B **246**, 2432–2435 (2009).

[180]J. Maultzsch, S. Reich, C. Thomsen, S. Webster, R. Czerw, D. Carroll, S. Vieira, P. Birkett, and C. A. Rego, "Raman characterization of boron-doped multiwalled carbon nanotubes," Appl. Phys. Lett. **81**, 2647–2649 (2002).
[181]S. G. Chou, H. Son, J. Kong, A. Jorio, R. Saito, M. Zheng, G. Dresselhaus, and M. S. Dresselhaus, "Length characterization of DNA-wrapped carbon nanotubes using Raman spectroscopy," Appl. Phys. Lett. **90**, 131109 (2007).
[182]C. Cooper, R. Young, and M. Halsall, "Investigation into the deformation of carbon nanotubes and their composites through the use of Raman spectroscopy," Composites Part A **32**, 401–411 (2001).
[183]N. Geblinger, A. Ismach, and E. Joselevich, "Self-organized nanotube serpentines," Nat. Nanotechnol. **3**, 195 (2008).
[184]N. Shadmi, A. Kremen, Y. Frenkel, Z. J. Lapin, L. D. Machado, S. B. Legoas, O. Bitton, K. Rechav, R. Popovitz-Biro, D. S. Galvao *et al.*, "Defect-free carbon nanotube coils," Nano Lett. **16**, 2152–2158 (2016).
[185]D. Nakar, G. Gordeev, L. D. Machado, R. Popovitz-Biro, K. Rechav, E. F. Oliveira, P. Kusch, A. Jorio, D. S. Galvão, S. Reich *et al.*, "Few-wall carbon nanotube coils," Nano Lett. **20**, 953–962 (2019).
[186]P. Corio, S. D. M. Brown, A. Marucci, M. A. Pimenta, K. Kneipp, G. Dresselhaus, and M. S. Dresselhaus, "Surface-enhanced resonant Raman spectroscopy of single-wall carbon nanotubes adsorbed on silver and gold surfaces," Phys. Rev. B **61**, 13202–13211 (2000).
[187]K. Kneipp, A. Jorio, H. Kneipp, S. D. M. Brown, K. Shafer, J. Motz, R. Saito, G. Dresselhaus, and M. S. Dresselhaus, "Polarization effects in surface-enhanced resonant Raman scattering of single-wall carbon nanotubes on colloidal silver clusters," Phys. Rev. B **63**, 081401 (2001).
[188]K. Kneipp, H. Kneipp, P. Corio, S. D. M. Brown, K. Shafer, J. Motz, L. T. Perelman, E. B. Hanlon, A. Marucci, G. Dresselhaus, and M. S. Dresselhaus, "Surface-enhanced and normal stokes and anti-stokes Raman spectroscopy of single-walled carbon nanotubes," Phys. Rev. Lett. **84**, 3470–3473 (2000).
[189]K. Kneipp, H. Kneipp, M. S. Dresselhaus, and S. Lefrant, "Surface-enhanced Raman scattering on single wall carbon nanotubes," Philos. Trans. Math. Phys. Eng. Sci. **362**, 2361–2373 (2004).
[190]K. Kneipp, H. Kneipp, I. Itzkan, R. R. Dasari, M. S. Feld, and M. S. Dresselhaus, "Nonlinear Raman probe of single molecules attached to colloidal silver and gold clusters," in *Optical Properties of Nanostructured Random Media*, Topics in Applied Physics, edited by V. M. Shalaev (Springer-Verlag, Berlin, 2002), Vol. 82, pp. 227–247.
[191]K. Kneipp, L. T. Perelman, H. Kneipp, V. Backman, A. Jorio, G. Dresselhaus, and M. S. Dresselhaus, "Coupling and scattering power exchange between phonon modes observed in surface-enhanced Raman spectra of single-wall carbon nanotubes on silver colloidal clusters," Phys. Rev. B **63**, 193411 (2001).
[192]A. Hartschuh, E. J. Sánchez, X. S. Xie, and L. Novotny, "High-resolution near-field Raman microscopy of single-walled carbon nanotubes," Phys. Rev. Lett. **90**, 095503 (2003).
[193]N. Hayazawa, T. Yano, H. Watanabe, Y. Inouye, and S. Kawata, "Detection of an individual single-wall carbon nanotube by tip-enhanced near-field Raman spectroscopy," Chem. Phys. Lett. **376**, 174–180 (2003).
[194]M. Liao, S. Jiang, C. Hu, R. Zhang, Y. Kuang, J. Zhu, Y. Zhang, and Z. Dong, "Tip-enhanced Raman spectroscopic imaging of individual carbon nanotubes with subnanometer resolution," Nano Lett. **16**, 4040–4046 (2016).
[195]L. G. Cançado, A. Hartschuh, and L. Novotny, "Tip-enhanced Raman spectroscopy of carbon nanotubes," J. Raman Spectrosc. **40**, 1420–1426 (2009).
[196]L. Cançado, A. Jorio, A. Ismach, E. Joselevich, A. Hartschuh, and L. Novotny, "Mechanism of near-field Raman enhancement in one-dimensional systems," Phys. Rev. Lett. **103**, 186101 (2009).
[197]R. V. Maximiano, R. Beams, L. Novotny, A. Jorio, and L. G. Cançado, "Mechanism of near-field Raman enhancement in two-dimensional systems," Phys. Rev. B **85**, 235434 (2012).
[198]L. G. Cançado, R. Beams, A. Jorio, and L. Novotny, "Theory of spatial coherence in near-field Raman scattering," Phys. Rev. X **4**, 031054 (2014).
[199]A. Jorio, N. S. Mueller, and S. Reich, "Symmetry-derived selection rules for plasmon-enhanced Raman scattering," Phys. Rev. B **95**, 155409 (2017).
[200]F. R. Pratama, M. S. Ukhtary, and R. Saito, "Non-vertical optical transition in near-field enhanced Raman spectroscopy of graphene," J. Phys. Condens. Matter **31**, 265701 (2019).
[201]M. Richard-Lacroix, Y. Zhang, Z. Dong, and V. Deckert, "Mastering high resolution tip-enhanced Raman spectroscopy: Towards a shift of perception," Chem. Soc. Rev. **46**, 3922–3944 (2017).
[202]Y. Okuno, Y. Saito, S. Kawata, and P. Verma, "Tip-enhanced Raman investigation of extremely localized semiconductor-to-metal transition of a carbon nanotube," Phys. Rev. Lett. **111**, 216101 (2013).
[203]S. Heeg, L. Shi, L. V. Poulikakos, T. Pichler, and L. Novotny, "Carbon nanotube chirality determines properties of encapsulated linear carbon chain," Nano Lett. **18**, 5426–5431 (2018).
[204]A. Jorio, L. G. Cançado, S. Heeg, L. Novotny, and A. Hartschuh, "Tip-enhanced spectroscopy and imaging of carbon nanomaterials," in *H*andbook of Carbon Nanomaterials (World Scientific, 2019), Vol. 9, pp. 175–221 .
[205]J. E. Riggs, Z. Guo, D. L. Carroll, and Y.-P. Sun, "Strong luminescence of solubilized carbon nanotubes," J. Am. Chem. Soc. **122**, 5879–5880 (2000).
[206]M. J. O'Connell, S. M. Bachilo, C. B. Huffman, V. C. Moore, M. S. Strano, E. H. Haroz, K. L. Rialon, P. J. Boul, W. H. Noon, C. Kittrell *et al.*, "Band gap fluorescence from individual single-walled carbon nanotubes," Science **297**, 593–596 (2002).
[207]R. B. Weisman and S. M. Bachilo, "Dependence of optical transition energies on structure for single-walled carbon nanotubes in aqueous suspension: An empirical Kataura plot," Nano Lett. **3**, 1235–1238 (2003).
[208]J. Lefebvre, J. Fraser, P. Finnie, and Y. Homma, "Photoluminescence from an individual single-walled carbon nanotube," Phys. Rev. B **69**, 075403 (2004).
[209]J. Maultzsch, R. Pomraenke, S. Reich, E. Chang, D. Prezzi, A. Ruini, E. Molinari, M. Strano, C. Thomsen, and C. Lienau, "Exciton binding energies in carbon nanotubes from two-photon photoluminescence," Phys. Rev. B **72**, 241402 (2005).
[210]J. Lefebvre, D. G. Austing, J. Bond, and P. Finnie, "Photoluminescence imaging of suspended single-walled carbon nanotubes," Nano Lett. **6**, 1603–1608 (2006).
[211]S. Ghosh, S. M. Bachilo, and R. B. Weisman, "Advanced sorting of single-walled carbon nanotubes by nonlinear density-gradient ultracentrifugation," Nat. Nanotechnol. **5**, 443–450 (2010).
[212]S. Kazaoui, N. Minami, R. Jacquemin, H. Kataura, and Y. Achiba, "Amphoteric doping of single-wall carbon-nanotube thin films as probed by optical absorption spectroscopy," Phys. Rev. B **60**, 13339 (1999).
[213]Y. Murakami, S. Chiashi, Y. Miyauchi, M. Hu, M. Ogura, T. Okubo, and S. Maruyama, "Growth of vertically aligned single-walled carbon nanotube films on quartz substrates and their optical anisotropy," Chem. Phys. Lett. **385**, 298–303 (2004).
[214]S. H. Jeong, K. K. Kim, S. J. Jeong, K. H. An, S. H. Lee, and Y. H. Lee, "Optical absorption spectroscopy for determining carbon nanotube concentration in solution," Synth. Met. **157**, 570–574 (2007).
[215]Z. Yu and L. Brus, "Rayleigh and Raman scattering from individual carbon nanotube bundles," J. Phys. Chem. B **105**, 1123–1134 (2001).
[216]M. Y. Sfeir, F. Wang, L. Huang, C.-C. Chuang, J. Hone, S. P. O'Brien, T. F. Heinz, and L. E. Brus, "Probing electronic transitions in individual carbon nanotubes by rayleigh scattering," Science **306**, 1540–1543 (2004).
[217]K. Liu, J. Deslippe, F. Xiao, R. B. Capaz, X. Hong, S. Aloni, A. Zettl, W. Wang, X. Bai, S. G. Louie *et al.*, "An atlas of carbon nanotube optical transitions," Nat. Nanotechnol. **7**, 325–329 (2012).
[218]S. Chiashi, Y. Murakami, Y. Miyauchi, and S. Maruyama, "Temperature dependence of Raman scattering from single-walled carbon nanotubes: Undefined radial breathing mode peaks at high temperatures," Jpn. J. Appl. Phys. **47**, 2010 (2008).
[219]A. S. Duarte, J. Rehbinder, R. R. Correia, T. Buckup, and M. Motzkus, "Mapping impurity of single-walled carbon nanotubes in bulk samples with multiplex coherent anti-stokes Raman microscopy," Nano Lett. **13**, 697–702 (2013).
[220]K. Watanabe, A. F. Palonpon, N. I. Smith, A. Kasai, H. Hashimoto, S. Kawata, K. Fujita *et al.*, "Structured line illumination Raman microscopy," Nat. Commun. **6**, 10095 (2015).

[221]U. Kajendirarajah, M. O. Avilés, and F. Lagugné-Labarthet, "Deciphering tip-enhanced Raman imaging of carbon nanotubes with deep learning neural networks," Phys. Chem. Chem. Phys. **22**, 17857–17866 (2020).
[222]R. Saito, K. Sato, P. Araujo, D. Mafra, and M. Dresselhaus, "Gate modulated Raman spectroscopy of graphene and carbon nanotubes," Solid State Commun. **175-176**, 18–34 (2013).
[223]W. Kohn, "Image of the fermi surface in the vibration spectrum of a metal (Kohn anomaly)," Phys. Rev. Lett. **2**, 393 (1959).
[224]E. H. Hasdeo, A. R. T. Nugraha, M. S. Dresselhaus, and R. Saito, "Fermi energy dependence of first- and second-order Raman spectra in graphene: Kohn anomaly and quantum interference effect," Phys. Rev. B **94**, 075104 (2016).
[225]K. Sasaki, H. Farhat, R. Saito, and M. S. Dresselhaus, "Kohn anomaly in Raman spectroscopy of single wall carbon nanotubes," Physica E **42**, 2005–2015 (2010).
[226]X. Wei, T. Tanaka, Y. Yomogida, N. Sato, R. Saito, and H. Kataura, "Experimental determination of excitonic band structures of single-walled carbon nanotubes using circular dichroism spectra," Nat. Commun. **7**, 12899 (2016).
[227]G. G. Samsonidze, R. Saito, A. Jorio, M. A. Pimenta, A. G. Souza Filho, A. Grüneis, G. Dresselhaus, and M. S. Dresselhaus, "The concept of cutting lines in carbon nanotube science," J. Nanosci. Nanotechnol. **3**, 431–458 (2003).
[228]N. Sato, Y. Tatsumi, and R. Saito, "Circular dichroism of single-wall carbon nanotubes," Phys. Rev. B **95**, 155436 (2017).
[229]H. Ajiki and T. Ando, "Physics of carbon nanotubes," Physica B **201**, 349 (1994).
[230]R. Saito, G. Dresselhaus, and M. S. Dresselhaus, "Trigonal warping effect of carbon nanotubes," Phys. Rev. B **61**, 2981–2990 (2000).
[231]S. G. Drapcho, J. Kim, X. Hong, C. Jin, S. Shi, S. Tongay, J. Wu, and F. Wang, "Apparent breakdown of Raman selection rule at valley exciton resonances in monolayer MoS_2," Phys. Rev. B **95**, 165417 (2017).
[232]Y. Tatsumi, T. Kaneko, and R. Saito, "Conservation law of angular momentum in helicity-dependent Raman and Rayleigh scattering," Phys. Rev. B **97**, 195444 (2018).
[233]A. Jorio, G. Dresselhaus, M. S. Dresselhaus, M. Souza, M. S. S. Dantas, M. A. Pimenta, A. M. Rao, R. Saito, C. Liu, and H. M. Cheng, "Polarized Raman study of single-wall semiconducting carbon nanotubes," Phys. Rev. Lett. **85**, 2617–2620 (2000).
[234]J.-H. Kim, A. Nugraha, L. Booshehri, E. Haroz, K. Sato, G. Sanders, K.-J. Yee, Y.-S. Lim, C. Stanton, R. Saito, and J. Kono, "Coherent phonons in carbon nanotubes and graphene," Chem. Phys. **413**, 55–80 (2013), Photophysics of carbon nanotubes and nanotube composites.
[235]J.-H. Kim, K.-J. Yee, Y.-S. Lim, L. G. Booshehri, E. H. Hároz, and J. Kono, "Dephasing of *G*-band phonons in single-wall carbon nanotubes probed via impulsive stimulated Raman scattering," Phys. Rev. B **86**, 161415 (2012).
[236]J.-H. Kim, K.-J. Han, N.-J. Kim, K.-J. Yee, Y.-S. Lim, G. D. Sanders, C. J. Stanton, L. G. Booshehri, E. H. Hároz, and J. Kono, "Chirality-selective excitation of coherent phonons in carbon nanotubes by femtosecond optical pulses," Phys. Rev. Lett. **102**, 037402 (2009).
[237]G. D. Sanders, C. J. Stanton, J.-H. Kim, K.-J. Yee, Y.-S. Lim, E. H. Hároz, L. G. Booshehri, J. Kono, and R. Saito, "Resonant coherent phonon spectroscopy of single-walled carbon nanotubes," Phys. Rev. B **79**, 205434 (2009).
[238]A. R. T. Nugraha, E. H. Hasdeo, and R. Saito, "Selective coherent phonon-mode generation in single-wall carbon nanotubes," J. Phys. Condens. Matter **29**, 055302 (2017).
[239]A. R. T. Nugraha, E. H. Hasdeo, G. D. Sanders, C. J. Stanton, and R. Saito, "Origin of coherent G-band phonon spectra in single-wall carbon nanotubes," Phys. Rev. B **91**, 045406 (2015).
[240]M. S. Dresselhaus, A. Jorio, M. Hofmann, G. Dresselhaus, and R. Saito, "Perspectives on carbon nanotubes and graphene Raman spectroscopy" Nano Lett. **10**, 751–758 (2010).
[241]M. S. Dresselhaus, G. Dresselhaus, and A. Jorio, "Raman spectroscopy of carbon nanotubes in 1997 and 2007," J. Phys. Chem. C **111**, 17887–17893 (2007).
[242]A. Jorio, R. Saito, G. Dresselhaus, and M. S. Dresselhaus "Determination of nanotubes properties by Raman spectroscopy," Philos. Trans. A Math. Phys. Eng. Sci. **362**(1824), 2311–2336 (2004).
[243]M. Souza, A. Jorio, C. Fantini, B. R. A. Neves, M. A. Pimenta, R. Saito, A. Ismach, E. Joselevich, V. W. Brar, Ge. G. Samsonidze, G. Dresselhaus, and M. S. Dresselhaus, "Single- and double-resonance Raman G-band processes in carbon nanotubes," Phys. Rev. B **69**, R15424 (2004).